hematopoietic cells from the bone marrow with retroviral vectors encoding either PAX5-C20orf112S or PAX5-C20orf112L. GFP-positive infected bone marrow cells were sorted by FACS and plated in media containing cytokines that are know to stimulate B cell differentiation (Fig. 3*F*). Murine hematopoietic cells infected with the empty vector showed abundant colonies (Fig. 3*G Left*), and 79% of the cells were B220 positive B cells (Fig. 3*G Upper Right*). In contrast, murine hematopoietic cells infected with either PAX5-C20orf112S or PAX5-C20orf112L formed very few colonies (Fig. 3*G Left*). Most of these colonies were GFP-negative (data not shown), suggesting that these PAX5-fusion proteins impaired B cell development from murine hematopoietic cells.

Discussion

In this study, we describe a paradigm for discovering fusion genes in malignancy by taking advantage of samples with unbalanced translocations and using high density SNP-chip analysis. This technique allows us to identify genes involved in translocations even if chromosomal analysis is not available, especially in solid tumors.

Steps to identify novel fusion genes using SNP chip analysis include (*i*) identify either a deletion or duplication that occurs within two genes; (*ii*) determine whether transcription of both genes is in the same direction; (*iii*) take advantage of ancillary tests such as standard chromosomal analysis or spectral karyotyping (14), which can grossly show that two chromosomes are fused; and (*iv*) design primers of candidate genes and perform RT-PCR to clone fusion genes. Rapid amplication of cDNA ends (RACE) (15) or long-distance PCR (12) also help the cloning of genes involved in translocations. In our SNP-chip data, a number of regions of segmental deletions or duplications were detected (9). Although some of them are simple deletions or duplications at the original sites of the chromosomes, the others are deletions that occurred during chromosomal translocations or when duplicated fragments were inserted into chromosomal sites other than the original region (data not shown). Therefore, data of chromosomal analysis help to define translocations, leading to identification of candidate genes in novel fusion genes.

Recently, Tomlins *et al.* found the fusion genes *TMPRSS2/ERG* and *TMPRSS2/ETV1* in prostate cancers by using expression microarray data (16). They focused on the genes *ERG* and *ETV1*, which are highly expressed in this cancer and examined levels of individual exons of these two genes (16). They found differences in expression of 5′ and 3′ regions of the genes, suggesting that these genes are fused to each other (16). In these fusion genes, the 5′ regions were replaced by the *TMPRSS2* gene, resulting in the differences in the expression of the 5′ and 3′ region of the *ERG/ETV1* genes (16). They also used SNP-chip analysis to identify these fusion genes and found a deletion of a genomic region between TMPRSS2 (21q22.3) and ERG (21q22.2), leading to fusion of these two genes (17). These new technologies, based on oligonucleotide microarrays and bioinformatics, will help to identify fusion genes in cancers.

Our study found that the *PAX5* gene was frequently fused to one of a variety of partner genes. PAX5 is a key transcription factor in the development of B cells (18, 19). We found that these PAX5 fusion proteins suppressed the function of wild-type PAX5 in a dominant-negative fashion and suppressed expression of downstream target genes of wild-type PAX5 in leukemic cells.

We found that when *PAX5* was joined to one of its fusion partner genes, its C-terminal end was replaced by one of the partner genes. Elimination of the C-terminal end of *PAX5* may play an important role in generation of a dominant negative form of mutated *PAX5*. In *in vitro* assays, PAX5-fusion proteins showed a similar affinity as wild-type PAX5 for the PAX5 recognition sequences. Although expression of several downstream targets of wild-type PAX5 was repressed by expression of PAX5-fusion proteins, others were not affected. Binding of transcription factors to DNA can be modulated by cofactors and/or neighboring transcription factors (20). Compared to PAX5, PAX5-fusion proteins may bind more strongly to some target genes and more weakly to others, depending on the contextual environment of the target genes.

Further, our data showed that PAX5-fusion protein inhibited B cell development of hematopoietic cells in a colony formation assay. This result may suggest that PAX5 fusion protein blocked differentiation of hematopoietic cells into mature B cells. PAX5-deficient mice have impairment of B cell differentiation (18). These data suggest that PAX5-fusion proteins may contribute to leukomegenesis by blocking B cell differentiation. It has been suggested that two distinct genetic abnormalities contribute to leukemogenesis in acute myelogenous leukemia (AML); one is mutations promoting cellular proliferation, for example *FLT3* or *RAS* mutations, and the other is mutations blocking differentiation, for example *PML-RARA* or *RUNX1-ETO* (21, 22). PAX5-fusion proteins may cooperate with unidentified mutations promoting cellular proliferation in the ALL cells.

Recently, Mullighan *et al.* have analyzed pediatric ALL samples by high density SNP-chips and found frequent abnormalities of *PAX5* gene (23). Their data also showed that PAX5 fusion products suppressed transcriptional activity of PAX5 in a dominant-negative fashion (23). In addition, other researcher have reported *PAX5* fusion genes, including *PAX5* fused to *ETV6* (12p13) (23, 24), *FOXP1* (3p14) (23), *ZNF521* (18q11) (23), *ELN* (7q11.23) (25), and *PML* (15q24) (26). We have found *PAX5* fused to either *ETV6*, *FOXP1*, *C20orf112* (20q11), or *AUTS2* (7q11.22).

In our study, the function of PAX5 was attenuated by the dominant-negative forms of the fusion products in B cell lineage ALL, suggesting that PAX5 behaves as a tumor suppressor in early B cells, and that impairment of its function can be associated with the development of ALL. In contrast, translocation of the *PAX5* gene to the enhancer region of the Ig heavy chain gene [t(9;14)(p13.2;q32)] or point mutations of the 5′ regulatory region of the *PAX5* gene leads to its overexpression, which is associated with B cell lineage lymphomas (27–29). Also, experimental overexpression of wild-type PAX5 can transform lymphocytes (30, 31). Therefore, an aberrant PAX5 may behave in a dominant-negative fashion at the pre-B stage of B cell development, resulting in ALL; its forced expression in a more mature B cell can lead to lymphoma. Our study showed that PAX5-fusion proteins blocked differentiation of B cells but did not transform them. B cells at different stages of differentiation may need alteration of distinct sets of pathways to transform. Why PAX5 can act as a tumor suppressor in ALL and as an oncoprotein in lymphoma is unclear. Further studies are needed to clarify the mechanism of this paradoxical phenomenon in carcinogenesis.

In summary, we identified multiple fusion genes in ALL by SNP-chip analysis, leading to the exploration of a B cell differentiation block as a contributing factor to the development of ALL. This methodology should help researchers to identify oncogenic fusion genes and explore the mechanism of tumorigenesis in other types of cancers as well.

Materials and Methods

Samples and DNA/RNA Preparation. SNP-chip was performed on 399 pediatric ALL patients consecutively enrolled in the ALL-BFM 2000 trial of the Berlin-Frankfurt-Münster (BFM) study at diagnosis and during remission (350 cases were B cell lineage ALL and 49 cases were T cell lineage ALL) (9). Detailed results of the SNP-chip analysis are published separately (9). The ALL-BFM 2000 study was approved by the local ethics committee. DNA and RNA were extracted from the ALL samples and cell lines by using standard techniques (32). Nalm 6, a human pre-B ALL cell line, was generously provided by Dr. G. Crook (Los Angeles Children's Hospital, Los Angeles, CA) and maintained in RPMI medium 1640 with 10% FBS.

SNP-Chip Analysis. SNP-chip of GeneChip Human mapping 50k array XbaI 240 and/or 250k Nsp were used for this study (Affymetrix Japan). Preparation of samples was reported previously (4, 5). The data were analyzed by CNAG program as previously described (4, 5). All 399 ALL samples and their matched control samples were analyzed by using 50K-SNP chip; selected cases with genomic abnormalities were also analyzed by using 250K SNP-chip.

RT-PCR. RT-PCR was performed by using ThermoScript RT-PCR Systems (Invitrogen) according to the manufacturer's protocol. The primers used for detection of *PAX5* fusion transcripts are listed in Table S2. Expression of PAX5 downstream target genes in Nalm 6 cells after transfection was examined by semiquantitative RT-PCR. The gene names and their primer sequences are listed in Table S3.

Reporter Gene Constructs and Expression Vectors. The PAX5 reporter gene construct with the luciferase gene and PAX5 binding region of the CD19 promoter, as well as the human PAX5 cDNA constructs, were kindly provided by Dr. M. Busslinger (Research Institute of Molecular Pathology, Vienna, Austria). PAX5-fusion constructs were generated by using PCR. All coding regions were ligated into the pcDNA3.1 vectors (Stratagene). Wild-type PAX5 cDNA was ligated into pMSCV vector (Clontech), and EGFP cDNA was ligated under the control of pGK promoter as a marker (pMSCV-GFP-wtPAX5). PAX5-C20orf112S and PAX5-C20orf112L cDNA sequences were also ligated into pMSCV-GFP vectors.

Transfection and Reporter Gene Assay. For reporter gene assays, pMSCV-GFP-wtPAX5 and pcDNA vectors encoding PAX5-fusion genes were cotransfected with the PAX5 reporter construct and pRL (*Renilla* luciferase) vector into 293T cells by using the Effecten transfection kit (Qiagen). Firefly and *Renilla* luciferase activities were measured with the Dual-Luciferase Reporter Assay System (Promega). Transfection into Nalm6 human pre-B cell ALL cell line was performed with Amaxa nucleofector. GFP-positive cells were sorted by using the MoFlo cell sorter (Dako). Detailed information about the procedure is described in *SI Text*.

Retrovirus Transduction into Murine Hematopietic Cells. Retrovirus containing pMSCV-GFP (empty), pMSCV-GFP-PAX5-C20orf112S, and pMSCV-GFP-PAX5-C20orf112L was generated. The retrovirus was transfected into murine bone marrow cells as previously reported (33). After the transfection, GFP-positive cells were sorted and plated into methylcellulose cultures (M3231; Stem Cell Technologies) as previously described (33). Surface antigens (CD43, B220, c-kit, and CD11b) of these GFP-positive cells were examined by using FACScan (Becton–Dickinson). Detailed information of the procedure is described in the *SI Text*.

Subcellular Fractionation of Proteins and EMSA. Forty-eight hours after transfection of vectors into 293T cells, the cells were subjected to subcellular fractionation with the CelLytic NuCLEAR Extraction Kit (Sigma-Aldrich). Detailed information of the procedure is described in the *SI Text*.

Purified nuclear proteins from the cells were also subjected to EMSA as previously reported (34). Detailed information of the procedure is described in the *SI Text*.

Chromatin Immunoprecipitation (ChIP) Assay. ChIP assay was performed with the Magna ChIP A kit from Millipore according to the manufacturer's protocol. pMSCV-GFP or pMSCV-GFP-C20orf112S were transfected into Nalm 6 cells as described above, and GFP-positive cells were sorted by MoFlo (Dako). Precipitated DNA was recovered and subjected to PCR to amplify the *BLK* promoter region and the 3′ end of the *BLK* gene (internal control). The primer sequences used for ChIP assay are listed in Table S4. Detailed information of the procedure is described in the *SI Text*.

ACKNOWLEDGMENTS. We thank Dr. M. Busslinger (Research Institute of Molecular Pathology, Vienna, Austria) for generously providing the CD19 promoter reporter construct and the human PAX5 cDNA. This study was supported by the Parker Hughes Fund and by grants from the National Institutes of Health. N.K. is supported by a fellowship from The Tower Cancer Research Foundation. H.P.K. holds the Mark Goodson Chair in Oncology Research at Cedars-Sinai and is a member of the Jonsson Cancer Center and the Molecular Biology Institute of the University of California, Los Angeles. This work was also supported by a grant-in-aid from the Department of Health, Welfare and Labor; by the Ministry of Education, Culture, Sports, Science and Technology (Japan); by European Union Grant FOOD-CT-2005-016320; by grants from the Deutsche Krebshilfe to Cambridge Research Biochemicals; and by the Fritz-Thyssen Foundation (C.S.). The ALL-BFM 2000 trial is supported by Grant 50-2698-Schr 1 of the Deutsche Krebshilfe.

1. Armstrong SA, Look AT (2005) Molecular genetics of acute lymphoblastic leukemia. *J Clin Oncol* 23:6306–6315.
2. Pui CH, Evans WE (2006) Treatment of acute lymphoblastic leukemia. *N Engl J Med* 354:166–178.
3. Pui CH, Relling MV, Downing JR (2004) Acute lymphoblastic leukemia. *N Engl J Med* 350:1535–1548.
4. Nannya Y, *et al.* (2005) A robust algorithm for copy number detection using high-density oligonucleotide single nucleotide polymorphism genotyping arrays. *Cancer Res* 65:6071–6079.
5. Yamamoto G, *et al.* (2007) Highly sensitive method for genomewide detection of allelic composition in nonpaired, primary tumor specimens by use of affymetrix single-nucleotide-polymorphism genotyping microarrays. *Am J Hum Genet* 81:114–126.
6. Lindblad-Toh K, *et al.* (2000) Loss-of-heterozygosity analysis of small-cell lung carcinomas using single-nucleotide polymorphism arrays. *Nat Biotechnol* 18:1001–1005.
7. Raghavan M, *et al.* (2005) Genome-wide single nucleotide polymorphism analysis reveals frequent partial uniparental disomy due to somatic recombination in acute myeloid leukemias. *Cancer Res* 65:375–378.
8. Lehmann S, *et al.* (2008) Molecular allelokaryotyping of early-stage, untreated chronic lymphocytic leukemia. *Cancer* 112:1296–1305.
9. Kawamata N, *et al.* (2008) Molecular allelokaryotyping of pediatric acute lymphoblastic leukemias by high resolution single nucleotide polymorphism oligonucleotide genomic microarray. *Blood* 111:776–784.
10. Lin YH, Shin EJ, Campbell MJ, Niederhuber JE (1995) Transcription of the blk gene in human B lymphocytes is controlled by two promoters. *J Biol Chem* 270:25968–25975.
11. Schebesta A, *et al.* (2007) Transcription factor Pax5 activates the chromatin of key genes involved in B cell signaling, adhesion, migration, and immune function. *Immunity* 27:49–63.
12. Delogu A, *et al.* (2006) Gene repression by Pax5 in B cells is essential for blood cell homeostasis and is reversed in plasma cells. *Immunity* 24:269–281.
13. Schröck E, Padilla-Nash H (2000) Spectral karyotyping and multicolor fluorescence in situ hybridization reveal new tumor-specific chromosomal aberrations. *Semin Hematol* 37:334–347.
14. Frohman MA, Dush MK, Martin GR (1988) Rapid production of full-length cDNAs from rare transcripts by amplification using a single gene-specific oligonucleotide primer. *Proc Natl Acad Sci USA* 85:8998–9002.
15. Cheng S, Fockler C, Barnes WM, Higuchi R (1994) Effective amplification of long targets from cloned inserts and human genomic DNA. *Proc Natl Acad Sci USA* 91:5695–5699.
16. Tomlins SA, *et al.* (2005) Recurrent fusion of TMPRSS2 and ETS transcription factor genes in prostate cancer. *Science* 310:644–648.
17. Perner S, *et al.* (2006) TMPRSS2:ERG fusion-associated deletions provide insight into the heterogeneity of prostate cancer. *Cancer Res* 66:8337–8341.
18. Urbanek P, Wang ZQ, Fetka I, Wagner EF, Busslinger M (1994) Complete block of early B cell differentiation and altered patterning of the posterior midbrain in mice lacking Pax5/BSAP. *Cell* 79:901–912.
19. Xie H, Ye M, Feng R, Graf T (2004) Stepwise reprogramming of B cells into macrophages. *Cell* 117:663–676.
20. Kumaran RI, Thakar R, Spector DL (2008) Chromatin dynamics and gene positioning. *Cell* 132:929–934.
21. Gilliland DG, Griffin JD (2002) The roles of FLT3 in hematopoiesis and leukemia. *Blood* 100:1532–1542.
22. Tenen DG (2003) Disruption of differentiation in human cancer: AML shows the way. *Nat Rev Cancer* 3:89–101.
23. Mullighan CG, *et al.* (2007) Genome-wide analysis of genetic alterations in acute lymphoblastic leukaemia. *Nature* 446:758–764.
24. Cazzaniga G, *et al.* (2001) The paired box domain gene PAX5 is fused to ETV6/TEL in an acute lymphoblastic leukemia case. *Cancer Res* 61:4666–4670.
25. Bousquet M, *et al.* (2007) A novel PAX5-ELN fusion protein identified in B cell acute lymphoblastic leukemia acts as a dominant negative on wild-type PAX5. *Blood* 109:3417–3423.
26. Nebral K, *et al.* (2007) Identification of PML as novel PAX5 fusion partner in childhood acute lymphoblastic leukaemia. *Br J Haematol* 139:269–274.
27. Busslinger M, Klix N, Pfeffer P, Graninger PG, Kozmik Z (1996) Deregulation of PAX-5 by translocation of the Emu enhancer of the IgH locus adjacent to two alternative PAX-5 promoters in a diffuse large-cell lymphoma. *Proc Natl Acad Sci USA* 93:6129–6134.
28. Iida S, *et al.* (1996) The t(9;14)(p13;q32) chromosomal translocation associated with lymphoplasmacytoid lymphoma involves the PAX-5 gene. *Blood* 88:4110–4117.
29. Pasqualucci L, *et al.* (2007) Hypermutation of multiple proto-oncogenes in B-cell diffuse large-cell lymphomas. *Nature* 412:341–346.
30. Anderson K, *et al.* (2007) Ectopic expression of PAX5 promotes self renewal of biphenotypic myeloid progenitors co-expressing myeloid and B-cell lineage associated genes. *Blood* 109:3697–3705.
31. Souabni A, Jochum W, Busslinger M (2007) Oncogenic role of Pax5 in the T-lymphoid lineage upon ectopic expression from the immunoglobulin heavy-chain locus. *Blood* 109:281–289.
32. Sambrook J, Russell DW (2001) *Molecular Cloning: A Laboratory Manual.* (Cold Spring Harbor Press, Cold Spring Harbor, NY). 3rd Ed.
33. Schwieger M, *et al.* (2002) AML1-ETO inhibits maturation of multiple lymphohematopoietic lineages and induces myeloblast trnsformation in syngergy with ICSBP deficiency. *J Exp Med* 196:1227–1240.
34. Sato H, Wang D, Kudo A (2001) Dissociation of Pax-5 from KI and KII sites during kappa-chain gene rearrangement correlates with its association with the underphosphorylated form of retinoblastoma. *J Immunol* 166:6704–6710.

blood

2008 111: 776-784
Prepublished online Sep 21, 2007;
doi:10.1182/blood-2007-05-088310

Molecular allelokaryotyping of pediatric acute lymphoblastic leukemias by high-resolution single nucleotide polymorphism oligonucleotide genomic microarray

Norihiko Kawamata, Seishi Ogawa, Martin Zimmermann, Motohiro Kato, Masashi Sanada, Kari Hemminki, Go Yamatomo, Yasuhito Nannya, Rolf Koehler, Thomas Flohr, Carl W. Miller, Jochen Harbott, Wolf-Dieter Ludwig, Martin Stanulla, Martin Schrappe, Claus R. Bartram and H. Phillip Koeffler

Blood (print ISSN 0006-4971, online ISSN 1528-0020), is published semimonthly by the American Society of Hematology, 1900 M St, NW, Suite 200, Washington DC 20036.

Molecular allelokaryotyping of pediatric acute lymphoblastic leukemias by high-resolution single nucleotide polymorphism oligonucleotide genomic microarray

Norihiko Kawamata,[1] Seishi Ogawa,[2] Martin Zimmermann,[3] Motohiro Kato,[2] Masashi Sanada,[2] Kari Hemminki,[4] Go Yamatomo,[2] Yasuhito Nannya,[2] Rolf Koehler,[5] Thomas Flohr,[5] Carl W. Miller,[1] Jochen Harbott,[6] Wolf-Dieter Ludwig,[7] Martin Stanulla,[3] Martin Schrappe,[8] Claus R. Bartram,[5] and H. Phillip Koeffler[1]

[1]Department of Hematology, Oncology, Cedars-Sinai Medical Center/University of California at Los Angeles School of Medicine; [2]Regeneration Medicine of Hematopoiesis, University of Tokyo, School of Medicine, Tokyo, Japan; [3]Department of Pediatric Hematology and Oncology, Children's Hospital, Hannover Medical School (MHH), Hannover, Germany; [4]Division of Molecular Genetic Epidemiology, German Cancer Research Center (DKFZ), Heidelberg, Germany; [5]Institute of Human Genetics, University of Heidelberg, Heidelberg, Germany; [6]Department of Pediatric Hematology and Oncology, Justus Liebig University, Gießen, Germany; [7]Department of Hematology, Oncology and Tumor Immunology, Robert-Rössle-Clinic at the HELIOS-Clinic Berlin-Buch, Charité, Berlin, Germany; and [8]Department of Pediatrics, University of Kiel, Kiel, Germany

Pediatric acute lymphoblastic leukemia (ALL) is a malignant disease resulting from accumulation of genetic alterations. A robust technology, single nucleotide polymorphism oligonucleotide genomic microarray (SNP-chip) in concert with bioinformatics offers the opportunity to discover the genetic lesions associated with ALL. We examined 399 pediatric ALL samples and their matched remission marrows at 50 000/250 000 SNP sites using an SNP-chip platform. Correlations between genetic abnormalities and clinical features were examined. Three common genetic alterations were found: deletion of *ETV6*, deletion of *p16INK4A*, and hyperdiploidy, as well as a number of novel recurrent genetic alterations. Uniparental disomy (UPD) was a frequent event, especially affecting chromosome 9. A cohort of children with hyperdiploid ALL without gain of chromosomes 17 and 18 had a poor prognosis. Molecular allelokaryotyping is a robust tool to define small genetic abnormalities including UPD, which is usually overlooked by standard methods. This technique was able to detect subgroups with a poor prognosis based on their genetic status. (Blood. 2008;111:776-784)

Introduction

Pediatric acute lymphoblastic leukemia (ALL) is the most common malignant disease in children.[1-3] ALL is a genetic disease resulting from accumulation of mutations of tumor suppressor genes and oncogenes.[1-3] Knowledge of these mutations can be of use for diagnosis, prognosis, and therapeutic clinical purposes, as well as to provide an overall understanding of the pathogenesis of ALL.[1-3] Identification of mutated genes in ALL has evolved with improvement in technology. A recent approach is single nucleotide polymorphism (SNP) analysis using an array-based technology[4,5] that allows identification of amplifications, deletions, and allelic imbalance, such as uniparental disomy (UPD [represents the doubling of the abnormal allele due to somatic recombination or duplication and loss of the other normal allele]).[6-8] However, since this technique detects allelic dosage, it cannot detect balanced translocations.

According to the HapMap publication, 9.2 million SNPs have been reported, and of these, 3.6 million have been validated.[9] Global genomic distribution of SNPs and its easy adaptability for high throughput analysis make them the target of choice to look for genomic abnormalities in ALL and other cancers.[5-7]

Recently, higher resolution SNP-chip (50 000-500 000 probes) has been developed for large-scale SNP typing.[4,10] With a large number of SNP probes, in combination with the algorithms specifically developed for copy number calculations, these SNP-chips enable genomewide detection of copy number changes.[11,12] The combination of SNP-chip technology, nucleotide sequencing, and bioinformatics allows the investigator to view the entire genome of ALL in an unbiased, comprehensive approach. Using SNP-chips, the chromosomal abnormalities can be evaluated at a very high resolution (molecular level: average distances of each probe are 47 kb and 5.8 kb in the 50 k/500 k arrays, respectively[4,10]), and allele-specific gene dosage level (gene dosage of paternal and maternal alleles) also can be analyzed in the whole genome.[11,12] Hence, we name this new technology "molecular allelokaryotyping."[12] In this study, we performed molecular allelokaryotyping on a very large cohort (399) of pediatric ALL samples to examine genomic abnormalities at high resolution. Further, we examined correlations between the genomic abnormalities detected by SNP-chip and clinical features, including prognosis.

Submitted May 1, 2007; accepted September 13, 2007. Prepublished online as *Blood* First Edition paper, September 21, 2007; DOI 10.1182/blood-2007-05-088310.

N.K., S.O., and M.Z. equally contributed to this work as first authors. C.R.B. and H.P.K. equally contributed to this work as last authors.

An Inside *Blood* analysis of this article appears at the front of this issue.

The online version of this article contains a data supplement.

The publication costs of this article were defrayed in part by page charge payment. Therefore, and solely to indicate this fact, this article is hereby marked "advertisement" in accordance with 18 USC section 1734.

Methods

Clinical samples and DNA/RNA preparation

The ALL-BFM 2000 trial of the Berlin-Frankfurt-Münster (BFM) study group on treatment of childhood ALL enrolled patients from ages 1 year to 18 years at diagnosis.

From September 1999 to January 2002, 566 patients were consecutively enrolled in this trial. The ALL-BFM 2000 study was approved by the ethics committees of the Medical School Hanover and the Cedar Sinai Medical Center. Informed consent was obtained in accordance with the Declaration of Helsinki.

Of the 566 patients (nos. 299-854), 399 patients, representing 70% of the entire patient population, had additional DNA available and could be included in the present SNP-chip study. The 167 patients not available for this analysis did not differ from the 399 patients in this study with regard to their clinical and biological characteristics (data not shown).

Complete remission (CR) was defined as the absence of leukemia blasts in the peripheral blood and cerebrospinal fluid, fewer than 5% lymphoblasts in marrow aspiration smears, and no evidence of localized disease. At day 29, bone marrows were examined, and all patients in this SNP-chip analysis study obtained a CR at that time. The remission marrows were collected and used as matched control for the SNP-chip analysis.

Prednisone response was defined based on numbers of peripheral blood blasts per microliter on day 8, and patients were classified into good (< 1000 blasts/μL) and poor responders (≥ 1000 blasts/μL).[13-15] Relapse was defined as recurrence of lymphoblasts or localized leukemic infiltrates at any site.

DNA index, immunophenotyping, molecular analysis of chromosomal abnormalities

Leukemic or normal bone marrow cells were stained with propidium iodide, and cellular DNA contents were measured by cytometric analysis as previously reported.[16,17] DNA index was defined as the DNA content of leukemic cells compared with normal G0/G1 cells. When the DNA index of leukemic cells was the same as or greater than 1.16, it was defined as hyperdiploid ALL by DNA index as previously reported.[16,17]

Immunophenotyping of ALL was examined using anti-CD2, -CD3, -CD4, -CD10, -CD19, and -CD20 antibodies by FACS.[13-15] ETV6/RUNX1, BCR/ABL, and MLL/AF4 were examined by interphase fluorescence in situ hybridization (FISH) analysis using specific probes and by reverse transcriptase–polymerase chain reaction (RT-PCR) using specific primers for these fusion transcripts as described previously.[13-15]

Molecular allelokaryotyping of leukemic cells

DNA from the 399 ALL samples as well as their paired normal DNA from remission samples were analyzed on Affymetrix GeneChip human mapping 50 K *Xba*I or 250 K Nsp arrays (Affymetrix Japan, Tokyo, Japan) according to the manufacturer's protocol. Microarray data were analyzed for determination of both total and allelic-specific copy numbers using the CNAG program as previously described[11,12] with minor modifications, where the status of copy numbers as well as UPD at each SNP was inferred using the algorithms based on Hidden Markov Models.[11,12]

For clustering of ALL samples with regard to the status of copy number changes as well as UPD, entire genome was divided into contiguous sub-blocks of 100 kb in length, and according to the inferred copy numbers (CNs) and the status of UPD, one of the 4 conditions was assigned to the *i*th sub-block (S*i*); CN gain, CN loss, normal CN, and UPD. For a given 2-copy number data, A and B, distance (d[A,B])was simply defined as

$$d(A,B) = \sum_i \mathrm{I}(S_i^A; S_i^B)$$

$$\mathrm{I}(S_i^A; S_i^B) = \begin{cases} 1 \text{ if } S_i^A = S_i^B \\ 0 \text{ if } S_i^A \neq S_i^B \end{cases}$$

where S_i^A and S_i^B are the status of the *i*th sub-block (S*i*) in data A and B, respectively, and sum is taken for all sub-blocks. Clustering was initiated by finding a seed cluster of 2 samples showing the minimum distance and replacing them with the cluster data having the mean S*i* value of the two. This procedure was iteratively performed until all samples were converged to one cluster based on this distance using a program developed for this purpose (GNAGraph), which was followed by manual revisions focusing on particular genetic lesions selected by their frequencies within the sample set. CNAG and CNAGraph are available on request.

Quantitative genomic PCR and direct sequencing

Quantitative genomic PCR (qPCR) was performed on a real-time PCR machine, iCycler (Bio-Rad Laboratories, Hercules, CA) using iQ cybergreen supermix (Bio-Rad Laboratories) according to the manufacturer's protocol. Primer sequences used for the qPCR are listed in Table S2 (available on the *Blood* website; see the Supplemental Materials link at the top of the online article). Gene dosage at the 2p allele was used as an internal control. Allelic gene dosage of 9p and 9q was measured, and these were compared with the levels in respective matched control DNA. SNP sites were amplified and directly sequenced on Autosequencer 3000 (Applied Biosystems, Foster City, CA). Primers used for SNP site amplification are listed in Table S2. Exons 12 and 14 of JAK2 gene were amplified as previously reported.[18] PCR products were purified and subjected to direct sequencing.

Data preparation

Proportional differences between groups were analyzed by either chi-squared (χ^2) or Fisher exact tests. The Kaplan-Meier method was used to

Table 1. Characterization of clinical features of 399 ALL cases

	Cases, no. (%)
Sex	
Male	230 (57)
Female	169 (43)
Age	
1 to 9 yrs	307 (77)
Older than 10 yrs	92 (23)
WBC	
Below $10^2 \times 10^9$/L	362 (91)
Over $10^2 \times 10^9$/L	37 (9)
Immunophenotype	
T-cell	49 (12)
B-cell	339 (85)
Unknown	11 (3)
CNS involvement	
Yes	11 (3)
No	358 (90)
unknown	30 (7)
BCR/ABL	
Yes	6 (2)
No	379 (95)
Unknown	14 (3)
ETV6/RUNX1	
Yes	96 (24)
No	270 (68)
Unknown	33 (8)
PDN response	
Good	360 (90)
Poor	35 (9)
Unknown	4 (1)

WBC indicates white blood cell count ($\times 10^9$/L) in peripheral blood at diagnosis; CNS involvement, central nervous system involvement at diagnosis; *BCR/ABL* and *ETV6/RUNX1*, *BCR/ABL* or *ETV6/RUNX1* fusion was examined by RT-PCR and/or FISH analysis; PDN, prednisone; and PDN response, blast cell count was 1000/μL or greater in peripheral blood after a 7-day exposure to prednisone and one intrathecal dose of methotrexate.

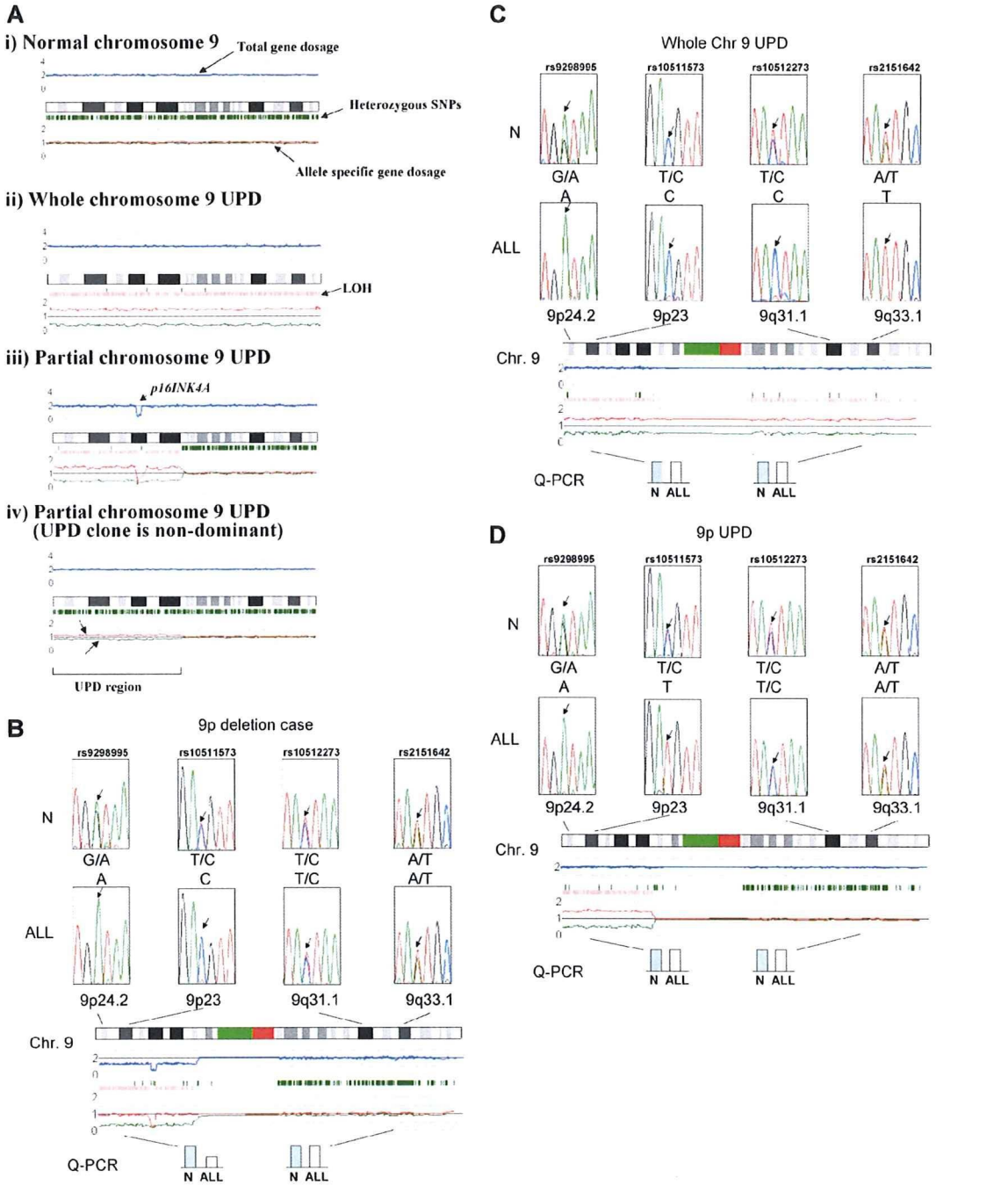

Figure 1. Result of SNP-chip analysis. (A) Results of normal and abnormal chromosomes visualized by CNAG software. Blue lines above each chromosome show total gene dosage; level 2 indicates diploid (2N) amount of DNA, which is normal. Green bars under each chromosome indicate the SNP sites showing heterozygosity in leukemic cells. When heterozygosity is not detected in the leukemic cells but is detected in matched normal controls, the result suggests that the leukemic cells have allelic imbalance (AI) in that region. Pink bars that replaced green ones suggest AI. The bottom lines (green and red lines) in each panel show allele-specific gene dosage levels (one indicates the gene dosage of paternal allele, the other indicates the gene dosage of maternal allele). Level 1 is normal for each gene dosage. (i) Pattern of normal chromosome 9. Blue line is at level 2 (2N DNA). Large number of SNP sites shows normal heterozygosity (green bars under the chromosomes), and no pink bars are detected. Allele-specific gene dosage is at level 1. Panel ii shows the pattern of whole chromosome 9 uniparental disomy (UPD) detected by SNP-chip. Total gene dosage (blue line) is normal (level 2). A number of pink bars (AI) are detected. Allele-specific gene dosage data show that one allele is deleted (level 0) and the other allele is duplicated (level 2). Panel iii shows the pattern of partial UPD. Left half shows the pattern of UPD as described above. Right half shows the pattern of a normal chromosome as described above. This case also has homozygous deletion of *p16INK4A* gene (see that both allele-specific dosage lines [green and red lines] and total gene dosage line [blue line] are at zero). Panel iv shows nondominant UPD. Total gene dosage (blue line) indicates 2N. Allele-specific gene dosage lines (arrows, green and red lines) on left half show that one allele (green line) is lower than normal, and the other allele (red line) is higher than normal. Allele-specific gene dosage on right half show that each allele has same level. (B-D) Validation of SNP-chip data by direct nucleotide sequencing of SNP sites and qPCR. Top panels: direct nucleotide sequencing of SNP sites in ALL samples with matched controls. ALL indicates leukemic samples; N, matched control samples. Heterozygous SNP sites are indicated by arrows. Middle panels: results of SNP-chip data (see Figure 1 legend). Bottom panels: qPCR at each chromosome location. Gene dosage levels were examined using qPCR at indicated chromosomal region. Gene dosage was determined relative to the levels at the 2p21 region. Gene dosage in leukemic cells (ALL) was compared with the matched normal control DNA (N). (B) ALL with 9p hemizygous deletion; homozygous deletion of 9p21 is also detected. (C) ALL with whole chromosome UPD. (D) ALL with 9p UPD.

Table 2. Detection of hyperdiploidy ALL by DNA-index and SNP-chip analysis

	SNP-chip	
	HD	non-HD
DNA index		
HD	44 cases	4 cases
non-HD	30 cases	200 cases

DNA index was measured by FACS as described in "DNA index, immunophenotyping, molecular analysis of chromosomal abnormalities" and DNA index of 278 ALL samples were available. Normal diploid cells have a DNA index of 1.0. When DNA index is the same as or greater than 1.16, the leukemia is defined as hyperdiploid ALL by DNA index. Hyperdiploid ALL detected by SNP-chip analysis had more than 50 chromosomes, which were counted manually.

HD indicates hyperdiploid ALL; and non-HD, nonhyperdiploid ALL.

estimate survival rates. Differences were compared with the 2-sided log-rank test. Event-free survival (EFS) was calculated from diagnosis to the time of the first event (relapse, secondary malignancy, or death from any cause) or to the date of last follow-up.

Results

Features of samples

Clinical features of 399 pediatric ALL patients are shown in Table 1. Infant ALL (< 1years of age) were excluded from this study, and 77% (307 cases) of the patients were from 1 to 9 years old. Forty-nine cases of T-cell lineage ALL and 339 cases of B-cell lineage ALL were examined. Ninety-six samples (24%) had *ETV6/RUNX1* fusion, and 6 cases had the *BCR/ABL* fusion gene.

Validation of SNP-chip data

Gene dosage, heterozygous SNPs, allele-specific gene dosage, and allelic composition (loss of heterozygosity [LOH]) was visualized as shown in Figure 1 using our novel analysis software, CNAG for SNP-chip.[11,12] Duplication/amplification, deletion, and UPDs of chromosomes were easily detected (Figure 1A). To validate abnormalities found by SNP-chip, genomic quantitative PCR and direct sequencing of SNP sites at duplicated, amplified, deleted, and UPD regions were performed including chromosome 9. Representative results of validation are shown in Figure 1B-D.

Also, hyperdiploid (HD) ALL defined by DNA index and SNP-chip analysis was compared for selected cases (Table 2). Number of total chromosomes was counted manually in SNP-chip analysis, and ALL with more than 50 chromosomes was defined as HD-ALL by SNP-chip. When DNA index of leukemic cells was same as or greater than 1.16, the sample was defined as HD-ALL by DNA index.[16,17] DNA index of 278 ALL samples were available, and 200 cases were defined as non-HD ALL by both methods. SNP-chip detected more cases of HD-ALL (74 cases) than DNA index. As shown in Figure 1Aiv, SNP-chip can precisely detect gene dosage, and this high sensitivity of SNP-chip analysis permitted more accurate detection of HD-ALL than by the DNA index method. Results of these analyses validated that the abnormalities detected by SNP-chip were reliable.

Three common abnormalities in pediatric ALL

Figure 2A summarizes molecular allelokaryotyping profiles of the 399 ALL cases after clustering with regard to the status of copy number alterations as well as copy number neutral LOH, so-called UPD, showing a number of clusters having common genetic lesions.

Among these clusters, 3 genetic abnormalities were frequently detected: hyperdiploidy (HD, > 50 chromosomes), deletion of the 9p region, and deletion of 12p (Figure 2A,B). The common deleted region (CDR) on 9p involved the *p16INK4A* gene (called p16Del, Figure 2B), and the CDR on 12p involved the *ETV6* gene (called ETV6Del, Figure 2B). Concurrent abnormalities of p16Del and HD were rare ($P < .001$); concurrent abnormalities of ETV6Del and HD also were rare ($P < .001$; Figure 2B). No case had all 3 common abnormalities.

The clinical features of cases with each of these 3 genetic abnormalities were analyzed (Table 3). Individuals with p16Del-ALL frequently were older ($P = .017$), had higher WBC ($P < .001$), and T-cell lineage ALL ($P < .001$). Those with ETV6Del-ALL were more often younger ($P = .009$), non–T-cell lineage ($P = .014$), and *ETV6/RUNX1* fusion gene positive ($P < .001$). Patients having HD-ALL were more frequently younger ($P < .001$), showed lower WBC ($P < .001$), non–T-cell lineage ($P < .001$), and *ETV6/RUNX1* negative ($P < .001$).

Numerical chromosomal abnormalities in pediatric ALL

Numerical chromosome changes were frequently detected in pediatric ALL samples, as summarized in Figure 3A. Numerical change of chromosome 21 (trisomy, tetrasomy, and pentasomy) was the most frequent (134 [34%] cases). We had 8 cases with Down syndrome who had trisomy 21 in their leukemic cells and their matched controls. These 8 cases are excluded in Figure 3A. Most of the numerical abnormalities were detected in HD-ALL cases (Figure S1A) except for those with trisomy 21 (Figure S1B). As for trisomy 21, half (21 cases) occurred in patients with subtypes other than HD (Figure S1B). In HD-ALL, gain of chromosomes was restricted to particular chromosomes, involving chromosomes 4, 6, 8, 10, 14, 17, 18, 21, and X (Figures 2A, 3A).

Nonrandom genetic abnormalities in pediatric ALL detected by SNP-chip

All copy number changes (deletions and duplications/amplifications) detected by SNP-chip analysis are shown in Figure 2A and Figure S2. Small deletions that could not be detected by conventional cytogenetics were sensitively identified, including deletions of 3p14.2 (500 kb), 3q26.32 (700 kb), and Xp21.1 (1 Mb) (Table 4 and Figure S2). Nonrandom chromosomal abnormalities (frequency > 1.5% of all cases) are listed in Table 4. Besides the 3 common genetic abnormalities, duplication of 1q (11%) and deletion of 6q (11.5%) were often detected. In 13 cases with 1q duplication, the duplication began at the *PBX1* gene (Figures 2A, S2). Since gain of the entire or part of either chromosome 21 or X was frequently found in non–HD-ALL, these abnormalities were grouped separately (Table 4).

Recently, other groups of investigators performed SNP-chip analysis on pediatric ALL and found deletions of several transcriptional factors associated with B-cell development including *PAX5* (9p13), *EBF* (5q33), *Ikaros* (7p12.2), *Aiolos* (17q12), *LEF1*(4q25), *RAG1*(11p12), and *RAG2* (11p12).[19,20] We also have found deletion of these genes in our study. However, the frequency of deletion of these genes, except for PAX5, was low (fewer than 2%) and/or the deleted regions contained multiple genes (Table 4; Figure S2 and data not shown).

UPD

One of the major advantages of SNP-chip analysis is capability of sensitive detection of UPD, even in samples suffering from small

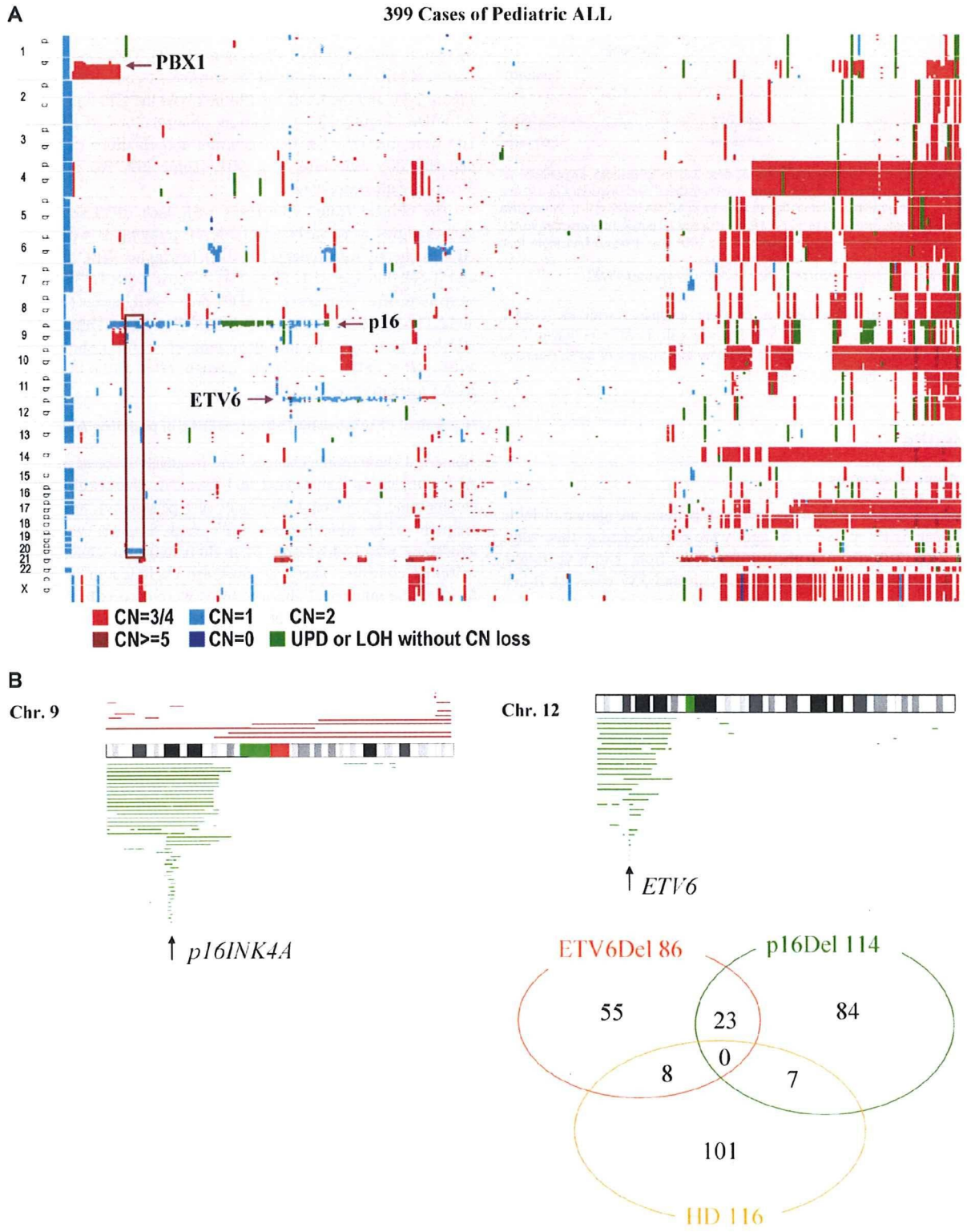

Figure 2. Allelokaryotyping of pediatric ALL. (A) Genetic clustering of 393 ALL samples. Genetic status of each chromosomal region is visualized. Vertical axis: chromosomes, p: short arms, q: long arms. Horizontal axis: individual cases. CN: copy number of alleles. UPD: uniparental disomy. Locations of *PBX1*, *INK4A/ARF*(p16), and *ETV6* genes are indicated. A rectangle indicates cases having 9p and 20q deletions. (B) Three common genomic abnormalities detected in ALL by SNP-chip analysis. Left panel: Deletion of 9p is frequently detected; the arrow indicates the commonly deleted region (CDR) where the p16INK4A gene is located. Right panel: Deletion of 12p often occurs. The arrow indicates that the CDR is where the ETV6 gene is localized. Green lines under the chromosome indicate the deleted regions in individual cases. Brown lines above the chromosome indicate the duplicated regions. Only representative cases are shown. Green and red bands on idiograms indicate centromeres and noncoding regions, respectively. Bottom panel: Venue diagram of 3 common abnormalities detected in this study. Numbers of respective cases in each category are indicated. HD: ALL with hyperdiploid (chromosomes > 50). ETV6Del: ALL with deletion of ETV6 gene. p16Del: ALL with deletion of p16INK4A gene.

Table 3. Clinical features of ALL cases associated with one of three common genetic abnormalities

	Genetic abnormality, no. (%)	Others, no. (%)	*P*
p16Del-ALL			
Age			
1 to 9 y	76 (68)	231 (80)	—
Older than 9 y	35 (32)	57 (20)	.017
WBC			
Below $10^2 \times 10^9$/L	85 (77)	277 (96)	—
Over $10^2 \times 10^9$/L	26 (23)	11 (4)	.001
Non-T lineage	71 (62)	263 (96)	—
T-lineage	83 (38)	11 (4)	.001
ETV6Del-ALL			
Age			
1 to 9 y	75 (87)	232 (74)	—
Older than 9 y	11 (13)	81 (26)	.009
Non-T lineage	89 (95)	261 (85)	—
T-lineage	4 (5)	45 (15)	.015
ETV6/RUNX1			
Positive	53 (66)	43 (15)	—
Negative	27 (34)	243 (85)	.001
HD-ALL			
Age			
1 to 9 y	101 (89)	206 (72)	—
Older than 9	13 (11)	79 (28)	.001
WBC			
Below $10^2 \times 10^9$/L	112 (98)	250 (88)	—
Over $10^2 \times 10^9$/L	2 (2)	35 (12)	.001
Non-T lineage	110 (100)	229 (82)	—
T-lineage	0 (0)	49 (18)	.001
ETV6/RUNX1	HD-ALL	Others	
Positive	8 (8)	88 (34)	—
Negative	97 (92)	173 (66)	.001

p16Del-ALL indicates ALL with deletion of *p16INK4A* gene; ETV6Del-ALL, ALL with deletion of *ETV6* gene; HD-ALL, ALL with hyperdiploidy (chromosomes >50); —, not applicable; WBC, white blood cell count in peripheral blood ($\times 10^9$/L) at diagnosis; *and ETV6/RUNX1, ETV6/RUNX1* fusion was examined by RT-PCR and/or FISH analysis.

tumor content; UPD in samples with as low as 20% of tumor contents are clearly identified (Figure 1Aiv). Whole and partial chromosome UPDs were observed in 95 cases; 6 cases showed both whole and partial chromosome UPD (Figure 3B). Most of the whole chromosome UPD was detected in HD-ALL (Figure 3C). UPD of whole chromosome 9 was the most common whole chromosome UPD (Figure 3B). In contrast, UPD involving part of chromosomes was most often found in non–HD-ALL cases (Figure 3C). Recurrent partial chromosome UPD was detected in many chromosomal regions (Figure 3B). We frequently found whole chromosome 9 UPD (18 cases) and 9p UPD (30 cases) (Figure 3B). *INK4A* deletion was often found in 9p UPD (23 of 30, 77%), while it was rare in whole chromosome 9 UPD (1 of 18, 6%) (Figure 3D).

Relationship between genetic abnormalities

Recurrent abnormalities described above were compared with each other (3 common abnormalities and 26 nonrandom alterations) to detect relationships between these abnormalities (Table S1). Strong correlations between abnormalities of 12p and 21q were detected, duplications of 12p and 21q often occurred simultaneously, and duplications of 21q were accompanied by deletion of the *ETV6* gene that was localized on 12p. ETV6Del ALL frequently had additional changes, including duplications (21q and 1q) and deletions (3p21, 1q, *FHIT*, 15q, and 4q). Abnormalities involving chromosome X, including *DMD* (Xp21.2) deletion, were frequently accompanied by deletions of 8p, 4q, and 6q. Deletion of 20q often occurred with either *p16INK4A* deletion or duplication of 21q (Figure 2A and Table S1).

Impact of nonrandom genetic abnormalities on prognosis

We analyzed prognosis of cases showing nonrandom abnormalities listed in Table 4 and found that the recurrent abnormalities had no impact on the event-free survival (EFS; data not shown) except for amplification/duplication of chromosome 9q. Our initial, early analysis found that EFS of pediatric ALL patients was not impacted by *ETV6* deletion either with or without *ETV6/RUNX1*. Nine cases with 9q amplification/duplication showed a poor prognosis (6 patients relapsed within 3 years; Figure S3A), although the number of cases having this abnormality is too small to reach a significant conclusion. Of these cases, 3 also had duplication of part of chromosome 22 (Figure S3B), suggesting that duplication of 9q is part of an extra copy of the Philadelphia chromosome. These 3 cases showed *BCR/ABL* positively by FISH/RT-PCR analysis (data not shown). Two other cases showed high copy number amplification that encompassed *ABL* and *NUP214* genes (Figure S3C), suggesting these cases had a *NUP214/ABL* fusion.[21] The ALL cells of these 2 cases were steroid-resistant and T-cell lineage phenotype.

Children with HD-ALL without gain of either chromosome 17 or 18 had a worse prognosis (Figure 4). Furthermore, children with HD-ALL and no extra copies of chromosomes 17 and 18 had a significantly worse prognosis ($P < .001$), with 53% EFS at 5 years compared with a 90% 5-year EFS in the other HD-ALL cohort (Figure 4).

Discussion

SNP-chip analysis is a reliable method to detect gene dosage, which was validated by direct sequencing of SNP sites and quantitative PCR in this study. To detect HD-ALL, DNA index is not a sensitive method since contaminated normal cells (DNA index 1.0) decrease the levels of DNA index of hyperdiploid leukemic cells. Although karyotyping is a good method to detect HD-ALL, sufficient number of high-quality chromosomal metaphases is not always obtained from the leukemic cells. SNP-chip analysis may be a more useful and reliable method to detect this subtype of ALL.

Molecular allelokaryotyping of a large series of pediatric ALL samples showed 3 major abnormalities: deletion of *p16INK4A*, deletion of *ETV6*, and hyperdiploidy. Besides these 3 common abnormalities, a number of novel, nonrandom changes were found in ALL. Some of them showed a very narrow commonly deleted region, which was limited to one target gene, including *FHIT* (3p14.2), *TBL1XR1* (3q26.3), and *DMD* (Xp21.2). *DMD* is the causative gene for Duchenne-type muscular dystrophy.[22] While germ-line inactivating mutations of this gene cause the disease, no association has been made between this disease and cancers, including ALL. Since *DMD* is an extremely large gene (2.4 Mb), deletion of it may occur as a result of instability of genomic DNA in ALL cells.

Other investigators and we have found in pediatric ALL a number of deleted genes, including transcriptional factors involved in B-cell differentiation.[19,20] However, since no point mutations of those genes, except PAX5, were detected,[19] it is unclear that these transcriptional factors associated with B-cell development are target genes of these deletions. Mullighan et al[19] and we have found that PAX5 gene is frequently involved in deletions and translocations (N.K., S.O., M.Z., et

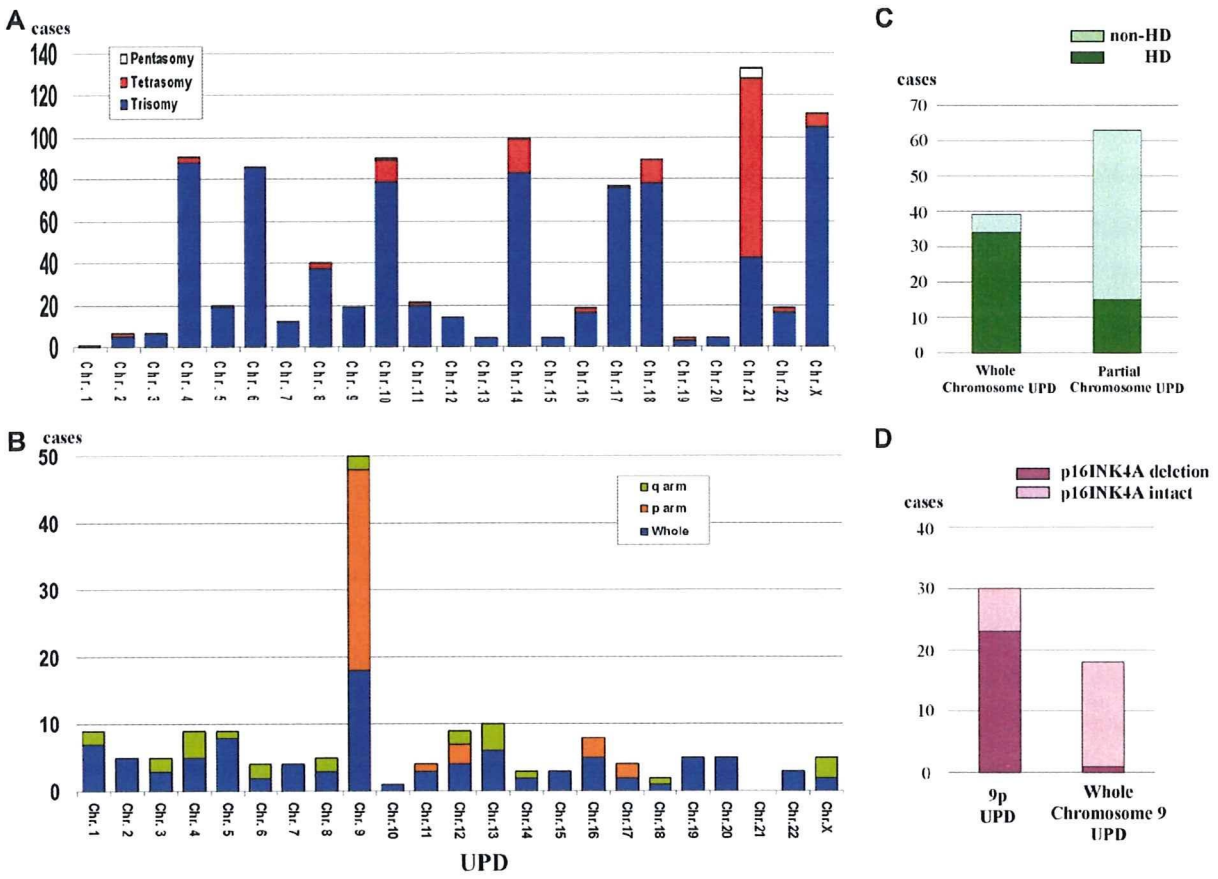

Figure 3. Numerical chromosomal changes and uniparental disomy in pediatric ALL. (A) Frequency of pentasomy/tetrasomy/trisomy affecting each chromosome. For X chromosome, trisomy (105 cases) contains trisosomy X in male pateints (67 cases) and disomy X in female patients (38 cases). All tetrasomy X were female patients. (B) Frequency of uniparental disomy (UPD). Whole: cases with whole chromosome UPD; p arm: cases with UPD of short arm; and q arm: cases with UPD of long arm. Chr: chromosome. UPD involving X chromosome was detected only in female cases. (C) Distribution of whole and partial chromosome UPD in HD and non–HD-ALL. Whole chromosome UPD is frequently detected in HD-ALL. Thirty-four cases with whole chromosome UPD were HD-ALL. Partial UPD is frequently detected in non–HD-ALL. Fifteen of 63 cases with partial UPD were HD-ALL. (D) Frequency of deletion of p16*INK4A* gene in whole chromosome 9 UPD and 9p UPD. Twenty-three cases showed deletion of p*16INK4A*, out of a total of 30 cases with 9p UPD. One case had p16*INK4A* deletion from a total 18 ALL samples with whole chromosome 9 UPD.

al, manuscript submitted), suggesting that impairment of PAX5 is associated with leukomogenesis.

This study showed that numerical chromosomal changes and UPD were common genomic abnormalities in pediatric ALL. Interestingly, whereas trisomy 21 was the most common numerical chromosomal abnormality, UPD of chromosome 21 was not detected in our study. Even in 8 cases with Down syndrome who had trisomy 21 in their constitutional DNA, UPD of chromosome 21 was not detected. Although UPD of chromosome 21 in leukemic cells of patients with Down syndrome has been reported,[8] it may be a rare event in pediatric ALL.

Chromosomal mis-segregation occurs when duplicated chromosomes separate improperly during cell division,[23] leading to numerical chromosomal changes in leukemic cells, including HD-ALL. Most of the whole chromosome UPD was detected in HD-ALL, suggesting that whole chromosome UPD is due also to chromosomal mis-segregation. In contrast, UPD involving part of chromosomes was most often found in non–HD-ALL cases. This may suggest that these partial UPDs are not caused by mis-segregation, but by mitotic recombination, which can usually cause chromosomal exchange.[24]

UPD involving chromosome 9 or 9p is a very common abnormality in pediatric ALL. *INK4A* gene may be a target gene of 9p UPD since most of the cases with 9p UPD had deletion of *INK4A* (23 of 30 cases with 9p UPD). For UPD involving whole chromosome 9, INK4A is not a target gene, since only one case with whole chromosome 9 UPD had deletion of this gene (1 of 18, 6%). Which gene is the target of whole chromosome 9 UPD is unclear. Furthermore, 7 cases with 9p UPD had intact *INK4A*, and the target gene of 9p UPD in these cases is also unknown. This is the first report showing that whole chromosome 9 UPD and 9p UPD are common abnormalities in pediatric ALL. Although Mullighan et al also analyzed a large number of pediatric ALL patients by SNP-chip,[19] they did not report this abnormality.

UPD on 9p is associated with activating point mutations of *JAK2* in myeloproliferative disorders (MPDs).[26-28] However, point mutation of *JAK2* in ALL is very rare.[29,30] We examined for *JAK2* mutations at "hot-spots" (exons 12 and 14)[18,26-28] in these 7 cases of ALL with 9p UPD in which deletion of *INK4A* was not detected. We found no mutations of *JAK2* in these cases. Another unidentified gene(s) in the region may be mutated in these cases.

In this study, we found that absence of gain of chromosomes 17 and 18 had an adverse impact on the prognosis of children with HD-ALL. Another large-scale study found that gain of chromosome 17 was associated with a better prognosis in HD-ALL.[31] Although this previous study reported that gain of chromosomes 4

Table 4. Recurrent genetic abnormalities detected by SNP-chip

Chromosomal sites	Type of abnormality	No. of cases (%)	Candidate genes
1q	Duplication	44 (11)	—
1q	Deletion	11 (3)	—
3p21	Deletion	6 (2)	—
3p14.2	Deletion	6 (2)	*FHIT*
3q26.3	Deletion	10 (3)	*TBL1XR1*
4q31	Deletion	7 (2)	—
6q	Deletion	46 (11)	—
7p	Deletion	10 (3)	—
7q34	Deletion	7 (2)	—
8p	Deletion	13 (3)	—
8q	Duplication	9 (2)	—
9q	Dup/amp	9 (2)	*ABL*
10p	Duplication	7 (2)	—
10q24	Deletion	12 (3)	—
11q	Deletion	24 (6)	—
12p	Duplication	13 (3)	—
13q14.2	Deletion	14 (4)	*RB1*
15q	Deletion	7 (2)	—
17p	Deletion	8 (2)	*TP53*
17q	Duplication	10 (3)	—
17q11.2	Deletion	7 (2)	*NF1*
20p12.2	Deletion	6 (2)	—
20q	Deletion	13 (3)	—
Xp21.2	Deletion	8 (2)	*DMD*
Gain of Chr. 21 or 21q in non-HD ALL cases	—	37/283 (13)	—
Gain of Chr. X or Xq in non-HD ALL cases	—	23/283 (8)	—

Nonrandom chromosomal abnormalities (frequency >1.5% of all cases) are listed. 9p deletion and 12p deletions are separately shown in Figure 2B.
HD indicates hyperdiploid (>50 chromosomes); dup/amp, duplication and amplification of the region; and —, not applicable.

and 10 also was associated with a better prognosis, our study showed that change in number of these chromosomes did not have an impact on prognosis. Even though the size of our study is relatively large, it might not be able to detect some important factors associated with survival because the number of cases of this ALL subtype enrolled in our study was too small or advances in treatment of pediatric ALL may have eliminated several factors that previously influenced prognosis.

One of the limitations of SNP-chip analysis is that it cannot detect balanced translocations, which are common abnormalities in ALL, since this technique can detect only allelic dosage. In our correlation study of genomic abnormalities, a strong correlation was found between abnormalities involving 12p and 21q as described above. This, in part, reflected translocations of chromosome 12p and 21q (*ETV6/RUNX1* fusion). Another correlation that we found between p16Del (on 9p) and deletion of 20q, may reflect dic(p13;q11).[9,20,32,33] These strong correlations of gains or loss of genetic materials may, therefore, sometimes suggest unbalanced translocations in ALL. Combination of SNP-chip and karyotyping will be a very strong technique to examine all genomic abnormalities in malignant cells.

Molecular allelokaryotyping of a series of 399 pediatric ALL samples has defined the range of genetic changes that occur in childhood ALL, including those associated with a poor prognosis. SNP-chip analysis is a novel technique that allows a thorough

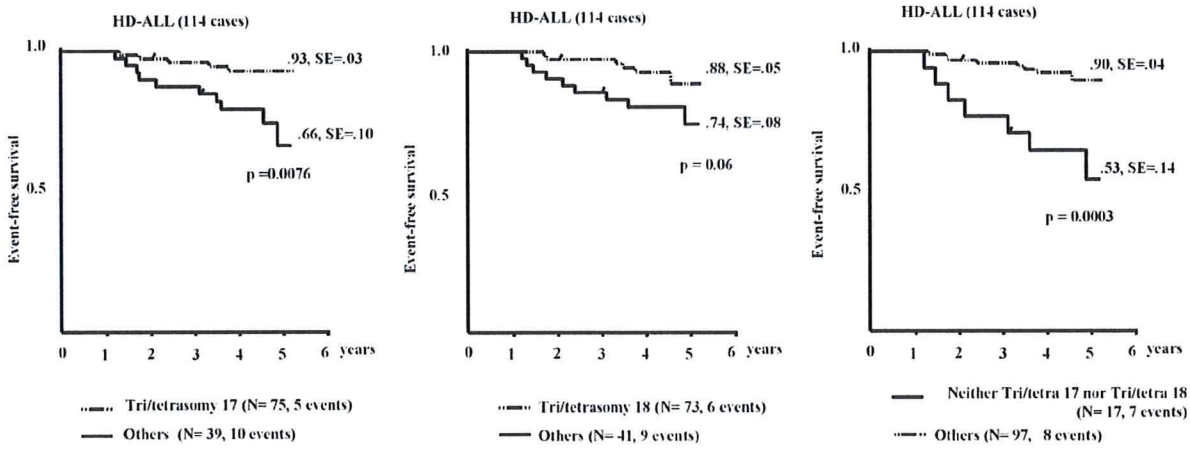

Figure 4. Prognostic impact of chromosomes 17 and 18. Absence of a gain of either chromosome 17 (left panel) or chromosome 18 (middle panel) is associated with poor prognosis in patients with HD-ALL; concurrent absence of a gain of both chromosomes 17 and 18 (right panel) is associated with very poor prognosis. Tri/tetra 18 and 17: HD-ALL with trisomy or tetrasomy 18 or 17. Others: HD-ALL without gain of chromosomes 17 and/or 18.

interrogation of the genome in ALL and identification of clinically significant subgroups of patients.

Acknowledgments

We thank the Parker Hughes Fund and National Institues of Health grants for supporting this study. N.K. is supported by the fellowship from The Tower Cancer Research Foundation. H.P.K. holds the Mark Goodson Chair in Oncology Research at Cedars Sinai and is a member of the Jonsson Cancer Center and the Molecular Biology Institute of UCLA. This work was also supported by grant-in-aid from Department of Health, Welfare. and Labor and from MEXT of the Japanese government, by EU grant FOOD-CT-2005-016320, and a grant from the Deutsche Krebshilfe to C.R.B. The ALL-BFM 2000 trial is supported by 50-2698-Schr 1 of the Deutsche Krebshilfe.

Authorship

Contribution: N.K. and S.O. designed this study, performed experiments, analyzed the data, and wrote the paper. M.Z., K.H., R.K., and W.-D.L. analyzed the data and wrote the paper. M.K., T.F., C.W.M., J.H., and M.S. analyzed the data. M.S., G.Y. and Y.N. performed experiments and analyzed the data. M.S. designed this study and wrote the paper. C.R.B. and H.P.K. designed this study, analyzed the data, and wrote the paper.

Conflict-of-interest disclosure: The authors declare no competing financial interests.

Correspondence: Seishi Ogawa, Department of Regeneration Medicine for Hematopoiesis, Graduate School of Medicine, University of Tokyo, 7-3-1 Hongo, Bunkyo-ku, Tokyo 113-8655, Japan; e-mail: sogawa-tky@umin.ac.jp; or Norihiko Kawamata, Hematology/Oncology, Cedars-Sinai Medical Institute, 8700 Beverly Blvd, Los Angeles, CA 90048; e-mail: kawamatan@cshs.org.

References

1. Armstrong SA, Look AT. Molecular genetics of acute lymphoblastic leukemia. J Clin Oncol. 2005;23:6306-6315.
2. Pui CH, Evans WE. Treatment of acute lymphoblastic leukemia. N Engl J Med. 2006;354:166-178.
3. Pui CH, Relling MV, Downing JR. Acute lymphoblastic leukemia. N Engl J Med. 2004;350:1535-1548.
4. Gunderson KL, Steemers FJ, Lee G, Mendoza LG, Chee MS. A genome-wide scalable SNP genotyping assay using microarray technology. Nat Genet. 2005;37:549-554.
5. Garraway LA, Widlund HR, Rubin MA, et al. Integrative genomic analyses identify MITF as a lineage survival oncogene amplified in malignant melanoma. Nature. 2005;436:117-122.
6. Raghavan M, Lillington DM, Skoulakis S, et al. Genome-wide single nucleotide polymorphism analysis reveals frequent partial uniparental disomy due to somatic recombination in acute myeloid leukemias. Cancer Res. 2005;65:375-378.
7. Teh MT, Blaydon D, Chaplin T, et al. Genomewide single nucleotide polymorphism microarray mapping in basal cell carcinomas unveils uniparental disomy as a key somatic event. Cancer Res. 2005;65:8597-8603.
8. Rogan PK, Close P, Blouin JL, et al. Duplication and loss of chromosome 21 in two children with Down syndrome and acute leukemia. Am J Med Genet. 1995;59:174-181.
9. International HapMap Consortium. A haplotype map of the human genome. Nature. 2005;437:1299-1320.
10. Matsuzaki H, Dong S, Loi H, et al. Genotyping over 100,000 SNPs on a pair of oligonucleotide arrays. Nat Methods. 2004;1:109-111.
11. Nannya Y, Sanada M, Nakazaki K, et al. A robust algorithm for copy number detection using high-density oligonucleotide single nucleotide polymorphism genotyping arrays. Cancer Res. 2005;65:6071-6079.
12. Yamamoto G, Nannya Y, Kato M, et al. Highly sensitive method for genomewide detection of allelic composition in nonpaired, primary tumor specimens by use of affymetrix single-nucleotide-polymorphism genotyping microarrays. Am J Hum Genet. 2007;81:114-126.
13. Bene MC, Castoldi G, Knapp W, et al. Proposals for the immunological classification of acute leukemias: European Group for the Immunological Characterization of Leukemias (EGIL). Leukemia. 1995;9:1783-1786.
14. Ludwig WD, Rieder H, Bartram CR, et al. Immunophenotypic and genotypic features, clinical characteristics, and treatment outcome of adult pro-B acute lymphoblastic leukemia: results of the German multicenter trials GMALL 03/87 and 04/89. Blood. 1998;92:898-909.
15. Schrappe M, Reiter A, Ludwig WD, et al. Improved outcome in childhood acute lymphoblastic leukemia despite reduced use of anthracyclines and cranial radiotherapy: results of trial ALL-BFM 90. German-Austrian-Swiss ALL-BFM Study Group. Blood. 2000;95:3310-3322.
16. Look AT, Melvin SL, Williams DL, et al. Aneuploidy and percentage of S-phase cells determined by flow cytometry correlate with cell phenotype in childhood acute leukemia. Blood. 1982;60:959-967.
17. Whitehead VM, Vuchich MJ, Lauer SJ, et al. Accumulation of high levels of methotrexate polyglutamates in lymphoblasts from children with hyperdiploid (greater than 50 chromosomes) B-lineage acute lymphoblastic leukemia: a Pediatric Oncology Group study. Blood. 1992;80:1316-1323.
18. Scott LM, Tong W, Levine RL, et al. JAK2 exon 12 mutations in polycythemia vera and idiopathic erythrocytosis. N Engl J Med. 2007;356:459-468.
19. Mullighan CG, Goorha S, Radtke I, et al. Genome-wide analysis of genetic alterations in acute lymphoblastic leukaemia. Nature. 2007;446:758-764.
20. Kuiper RP, Schoenmakers EF, van Reijmersdal SV, et al. High-resolution genomic profiling of childhood ALL reveals novel recurrent genetic lesions affecting pathways involved in lymphocyte differentiation and cell cycle progression. Leukemia. 2007;21:1258–1266.
21. Graux C, Cools J, Melotte C, et al. Fusion of NUP214 to ABL1 on amplified episomes in T-cell acute lymphoblastic leukemia. Nat Genet. 2004;36:1084-1089.
22. Koenig M, Hoffman EP, Bertelson CJ, Monaco AP, Feener C, Kunkel LM. Complete cloning of the Duchenne muscular dystrophy (DMD) cDNA and preliminary genomic organization of the DMD gene in normal and affected individuals. Cell. 1987;50:509-517.
23. Kops GJ, Weaver BA, Cleveland DW. On the road to cancer: aneuploidy and the mitotic checkpoint. Nat Rev Cancer. 2005;5:773-785.
24. Kotzot D. Complex and segmental uniparental disomy (UPD): review and lessons from rare chromosomal complements. J Med Genet. 2001;38:497-507.
25. Baxter EJ, Scott LM, Campbell PJ, et al. Acquired mutation of the tyrosine kinase JAK2 in human myeloproliferative disorders. Lancet. 2005;365:1054-1061.
26. James C, Ugo V, Le Couedic JP, et al. A unique clonal JAK2 mutation leading to constitutive signalling causes polycythaemia vera. Nature. 2005;434:1144-1148.
27. Kralovics R, Passamonti F, Buser AS, et al. A gain-of-function mutation of JAK2 in myeloproliferative disorders. N Engl J Med. 2005;352:1779-1790.
28. Levine RL, Wadleigh M, Cools J, et al. Activating mutation in the tyrosine kinase JAK2 in polycythemia vera, essential thrombocythemia, and myeloid metaplasia with myelofibrosis. Cancer Cell. 2005;7:387-397.
29. Levine RL, Loriaux M, Huntly BJ, et al. The JAK2V617F activating mutation occurs in chronic myelomonocytic leukemia and acute myeloid leukemia, but not in acute lymphoblastic leukemia or chronic lymphocytic leukemia. Blood. 2005;106:3377-3379.
30. Sulong S, Case M, Minto L, Wilkins B, Hall A, Irving J. The V617F mutation in Jak2 is not found in childhood acute lymphoblastic leukaemia. Br J Haematol. 2005;130:964-965.
31. Sutcliffe MJ, Shuster JJ, Sather HN, et al. High concordance from independent studies by the Children's Cancer Group (CCG) and Pediatric Oncology Group (POG) associating favorable prognosis with combined trisomies 4, 10, and 17 in children with NCI Standard-Risk B-precursor Acute Lymphoblastic Leukemia: a Children's Oncology Group (COG) initiative. Leukemia. 2005;19:734-740.
32. Rieder H, Schnittger S, Bodenstein H, et al. dic(9;20): a new recurrent chromosome abnormality in adult acute lymphoblastic leukemia. Genes Chromosomes Cancer. 1995;13:54-61.
33. Heerema NA, Maben KD, Bernstein J, Breitfeld PP, Neiman RS, Vance GH. Dicentric (9;20)(p11;q11) identified by fluorescence in situ hybridization in four pediatric acute lymphoblastic leukemia patients. Cancer Genet Cytogenet 1996;92:111-115.

Oncogene (2008) 27, 741–754

www.nature.com/onc

ORIGINAL ARTICLE

Stress via p53 pathway causes apoptosis by mitochondrial Noxa upregulation in doxorubicin-treated neuroblastoma cells

K Kurata[1], R Yanagisawa[1], M Ohira[2], M Kitagawa[3], A Nakagawara[2] and T Kamijo[1,2]

[1]Department of Pediatrics, Shinshu University School of Medicine, Matsumoto, Nagano, Japan; [2]Division of Biochemistry, Chiba Cancer Center Research Institute, Chuoh-ku, Chiba, Japan and [3]Department of Biochemistry, Hamamatsu University School of Medicine, Hamamatsu, Shizuoka, Japan

In this study, we employed a panel of cell lines to determine whether p53-dependent cell death in neuroblastoma (NB) cells is caused by apoptotic cellular function, and we further studied the molecular mechanism of apoptosis induced via the p53-dependent pathway. We obtained evidence that a type of p53-dependent stress, doxorubicin (Doxo) administration, causes accumulation of p53 in the nucleus of NB cells and phosphorylation of several serine residues in both Doxo-sensitive and -resistant cell lines. Upregulation of p53-downstream molecules in cells and upregulation of Noxa in the mitochondrial fraction were observed only in Doxo-sensitive NB cells. Significance of Noxa in the Doxo-induced NB cell death was confirmed by Noxa-knockdown experiments. Mitochondrial dysfunction, including cytochrome-*c* release and membrane potential disregulation, occurred and resulted in the activation of the intrinsic caspase pathway. However, in the Doxo-resistant cells, the accumulation in the nucleus and phosphorylation of p53 did not induce p53-downstream $p21^{Cip1/Waf1}$ expression and the Noxa upregulation, resulting in the retention of the mitochondrial homeostasis. Taken together, these findings indicate that the p53 pathway seems to play a crucial role in NB cell death by Noxa regulation in mitochondria, and inhibition of the induction of p53-downstream effectors may regulate drug resistance of NB cells.
Oncogene (2008) **27**, 741–754; doi:10.1038/sj.onc.1210672; published online 20 August 2007

Keywords: neuroblastoma; p53; noxa; mitochondria; apoptosis

Introduction

Neuroblastoma (NB) is the most common pediatric solid malignant tumor derived from the sympathetic nervous system. Unlike the many childhood malignancies for which survival has been improved by recent therapies, high-risk NB is still one of the most difficult tumors to cure, with only 30% long-term survival despite intensive multimodal therapy. New treatments and a better understanding of drug resistance mechanisms are required for the improvement of the survival rate. A noteworthy finding of NB research is that mutations of p53 tumor suppressor have been reported in less than 2% of NBs out of 340 tested (Tweddle *et al.*, 2001). Instead of mutation, cytoplasmic sequestration of p53 has been proposed as an alternative mechanism of inactivation in NB cells. The sequestration was first detected in frozen tumor samples using immunohistochemical techniques (Moll *et al.*, 1995) and later in NB cell lines by immunofluorescence and cell fractionation experiments (Moll *et al.*, 1996). However, several groups reported nuclear p53 accumulation in NB cells harboring wild-type p53 after DNA damage (Tweddle *et al.*, 2003). After nuclear accumulation, p53 phosphorylation, binding to targeted sequences and transcriptional transactivation are sequentially induced by DNA damage in *p53* wild-type cells (Oren, 1999). However, these processes in NB cells harboring wild-type p53 have not been examined with respect to the role of p53 pathways in the tumorigenesis of NB. Their examination should also yield insights into the molecular mechanisms of p53 inactivation. For instance, upregulation of the p53-downstream genes encoding $p21^{Cip1/Waf1}$ and HDM2 in *p53* wild-type NB cell lines was observed in several studies (Isaacs *et al.*, 2001; Keshelava *et al.*, 2001; Tweddle *et al.*, 2001) but not all (Wolff *et al.*, 2001). Reporter gene assays detected p53 transcriptional function in one study (Keshelava *et al.*, 2001) but not in another (Wolff *et al.*, 2001). Together, these facts indicate that systematic and detailed analysis of the biological effects of p53-dependent stress on the cell death of NB cells and of the mechanisms of activation and signal transduction of p53-related pathways in NB cells are required for understanding the mechanism of drug resistance and for the development of new therapies for high-risk NB patients.

The Bcl-2 family member proteins regulate mitochondrial cell death by controlling mitochondrial outer membrane permeabilization (MOMP). Anti-apoptotic Bcl-2 family members (for example, Bcl-2, Bcl-xL, Bcl-w and Mcl-1) function to block MOMP, whereas the

Correspondence: Dr T Kamijo, Division of Biochemistry, Chiba Cancer Center Research Institute, 666-2 Nitona, Chuoh-ku, Chiba 260-8717, Japan.
E-mail: tkamijo@chiba-cc.jp
Received 4 December 2006; revised 1 June 2007; accepted 11 June 2007; published online 20 August 2007

various pro-apoptotic proteins promote it. The pro-apoptotic proteins fall into two general subfamilies, based on the sharing of Bcl-2 homology domains. BH123 proteins appear to be effectors of MOMP, because cells from mice lacking the two major BH123 proteins, Bax and Bak, fail to undergo MOMP in response to a wide range of apoptotic stresses (Wei *et al.*, 2001). The other subfamily, the BH3-only proteins, can act either to activate Bax or Bak or to interfere with the anti-apoptotic Bcl-2 family members (Letai *et al.*, 2002). Noxa is a BH3-only member of Bcl-2 family proteins (Oda *et al.*, 2003) and its expression is induced by DNA damage such as that caused by etoposide or doxorubicin in a p53-dependent manner (Oda *et al.*, 2003; Shibue *et al.*, 2003). Furthermore, several lines of evidence reported that Noxa is one of the most important cell death effectors in neuronal cell death, for example, nuclear factor-kappa B modulated cell death in mouse cortical neurons (Aleyasin *et al.*, 2004), axotomized motor neurons of adult mouse (Kiryu-Seo *et al.*, 2005), sensory neurons especially in trigeminal ganglia and cervical dorsal ganglia (Hudson *et al.*, 2005) and arsenite-induced cortical neurons (Wong *et al.*, 2005).

These results have led us to study the role and molecular machinery of p53-dependent cell death in NB by utilizing several *p53* wild-type NB cell lines. We studied the sensitivities of NB cell lines to doxorubicin (Doxo), which is a representative cytotoxic drug against NB cells (Matthay *et al.*, 1998) that induces stresses that are basically dependent on p53 (Lowe *et al.*, 1994), and transactivates p53 and its downstream effectors in many tissues (Komarova *et al.*, 1997). In sensitive NB cells, the following important findings were observed after Doxo treatment: (1) accumulation of p53 in the nucleus; (2) activation of the p53-downstream molecules; (3) pro-apoptotic BH3-only Bcl-2 family protein Noxa induction and upregulation in mitochondria resulting in mitochondrial dysfunction/intrinsic caspase-derived apoptosis. Although p53 accumulated in the nucleus before Doxo treatment, the downstream molecules were not induced and the upregulation of Noxa in mitochondria was not observed in the Doxo-resistant NB cells. Consequently, the crucial role of the p53 pathway in apoptosis in NB cells was indicated by our observations.

Results

Heterogeneity of response to p53-dependent death signals in NB cell lines harboring wild-type p53

We chose 0.5 μg/ml of Doxo as an appropriate concentration to assess the effect of Doxo on NB cells according to the results of the analysis of peak plasma concentrations of doxorubicin (Hempel *et al.*, 2002). Similar results were obtained by 0.3–1.0 μg/ml of Doxo in the following experiments (data not shown). Trypan blue uptake assays were performed to compare the Doxo sensitivity of NB cell lines harboring wild-type *p53* (Figure 1a). More than 60% of cells were Trypan blue-positive for the SH-SY5Y, NB9, NB69 and SK-N-SH NB cell lines 36 h after Doxo stimulation. On the other hand, less than 40% of cells were positive in NB-19 and NB1 cell lines and less than 10% in IMR32 cells even 36 h after Doxo stimulation.

Next, we performed WST-8 assay, a modification of MTT assay, to evaluate cytotoxicity on NB cells (Figure 1b). We confirmed the sensitivity of NB cells to Doxo by these experiments and also studied the effects of etoposide, the other p53-dependent damage-inducing reagent, on NB cells. Etoposide was effectively cytotoxic on the Doxo-sensitive SK-N-SH, SH-SY5Y, NB-9 and NB-69 cells. In the Doxo-resistant NB cells, IMR32 and NB-1 cells also possessed drug resistance against etoposide, whereas NB-19 cells had sensitivity.

FACS analysis of sub-G_0/G_1 cells showed that considerable percentages of cells underwent apoptosis 24 h after the Doxo treatment in SH-SY5Y, NB-9, NB-69 and SK-N-SH (Figure 1c). However, the proportions of apoptotic cells were significantly lower in NB-19, NB-1 and IMR32 than in the four Doxo-sensitive NB cell lines. In SK-N-SH and SH-SY5Y cells, the increase of the sub-G_0/G_1 fraction after Doxo treatment was confirmed by the condensation and fragmentation of nuclei (Figure 1d). In contrast, almost all of the nuclei were intact in the resistant IMR32 and NB-1 cells. Thus, Doxo-induced stresses resulted in apoptosis in some NB cells, whereas others were resistant (Figure 1).

Upregulation and nuclear accumulation of p53 are not enough to induce apoptosis by Doxo treatment

To study the basis of the different sensitivities of NB cells to p53-dependent stress, we first performed direct western blot analysis using a monoclonal antibody recognizing the p53 N terminus (DO1) to estimate the total amount of p53. We also used antibodies that specifically react with phosphorylated serine residues (Ser15, Ser20 and Ser46) to examine the modulation of the stability and/or activity of p53 in response to DNA damage.

The amount of p53 was clearly increased by Doxo in the Doxo-sensitive NB cells, as detected with DO1 antibody (Figure 2a). p53 accumulation was observed in the Doxo-resistant IMR32 and NB-19 cells before treatment; serine15 phosphorylation was induced in all the NB cells after Doxo exposure. Upregulation of serine46 phosphorylation was also observed in the NB cell lines, except for IMR32 and SH-SY5Y cells. On the other hand, ser20 phosphorylation was not strongly upregulated in any of the lines. Consistent with previous reports, RT–PCR analysis showed that the induction of p53 protein by Doxo treatment in sensitive-NB cells was not caused at the transcriptional level (Figure 2b). Thus, it appears that the upregulation of p53 protein in Doxo-treated NB cells seemed to be caused by protein stabilization.

Next, we investigated the localization of p53 in NB cells, using DO1 as a human p53-specific antibody reacting with amino acids 21–25, pAb421 as a pan-p53 antibody reacting with the human p53 amino acids 370–378 and

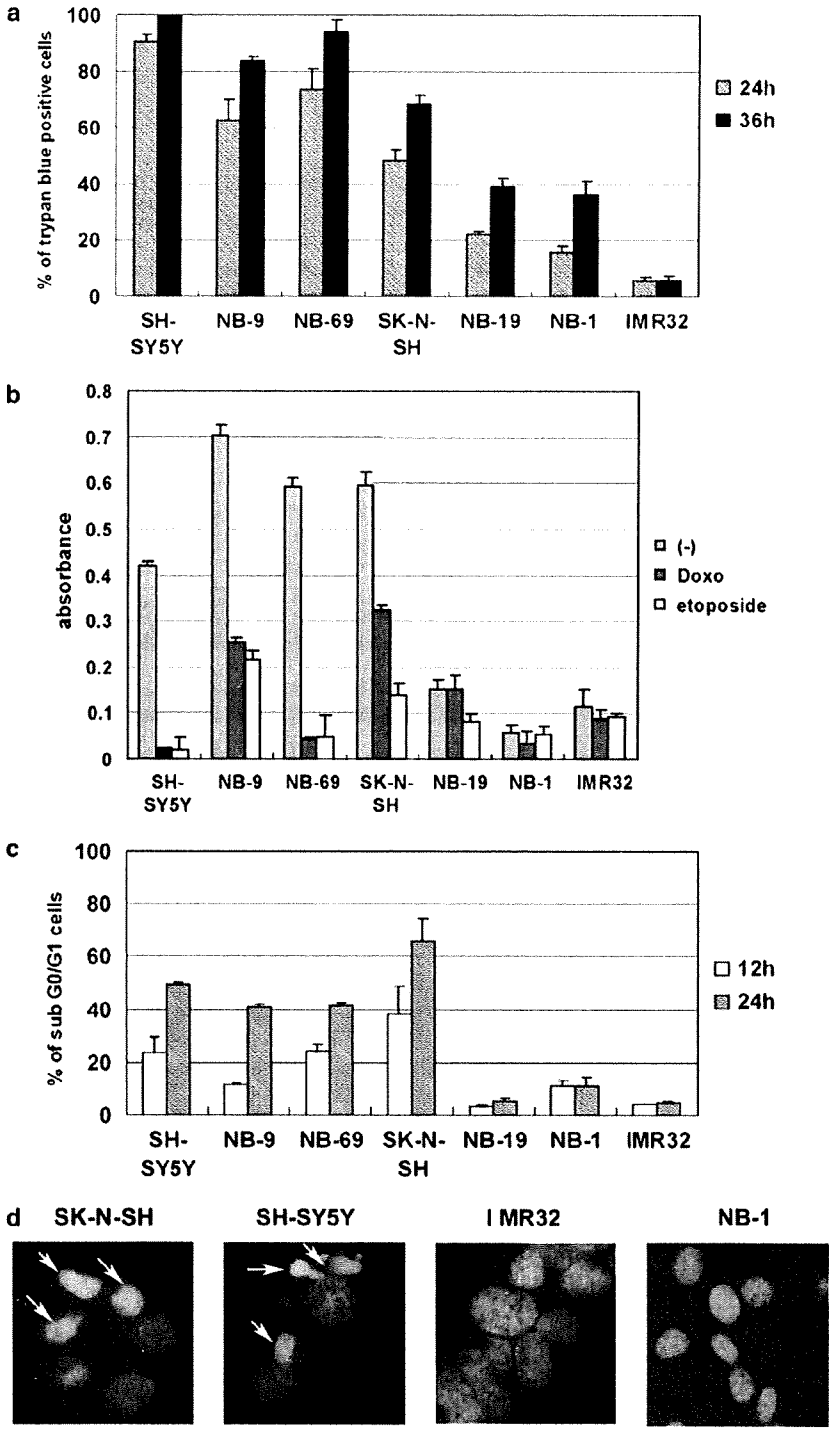

Figure 1 Sensitivity to doxorubicin (Doxo) is heterogenic in wild-type p53 harboring neuroblastoma (NB) cells. One hundred thousand cells were plated in a 3-cm-diameter culture dish and cultured in 5% CO_2 for 24 h. Doxo was added to the dish at 0.5 μg/ml and the incubation was continued for the indicated times. Mean and standard deviation (s.d.) of the % of cells were calculated for triplicate samples. (**a**) Cells were washed with 1 × phosphate-buffered saline (PBS), collected by 1 × PBS/0.5 mM EDTA, and stained with Trypan blue. The results are representative of four independent experiments. (**b**) After treatment of DNA-damaging reagents, cell viabilities were analysed by WST-8 assay. The results are representative of at least three independent experiments. (**c**) Analysis of the sub-G_0/G_1 fraction was performed as described in Materials and methods. The results are representative of three independent experiments. (**d**) Staining with 4′,6-diamidino-2-phenylindole (DAPI) was performed 24 h after Doxo stimulation. Arrows indicate the condensed or fragmented nuclei.

16G8 as an anti-phosphorylated p53ser15 antibody. Staining with pAb421 antibody revealed that the punctate cytoplasmic signal was upregulated in both Doxo-sensitive and -resistant NB cells after Doxo exposure (Figure 2c). DO1 antibody showed both nuclear and cytoplasmic staining before treatment, and remarkable accumulation into the nucleus was induced by Doxo in these four NB cell lines. Although ser15 phosphorylation was hardly

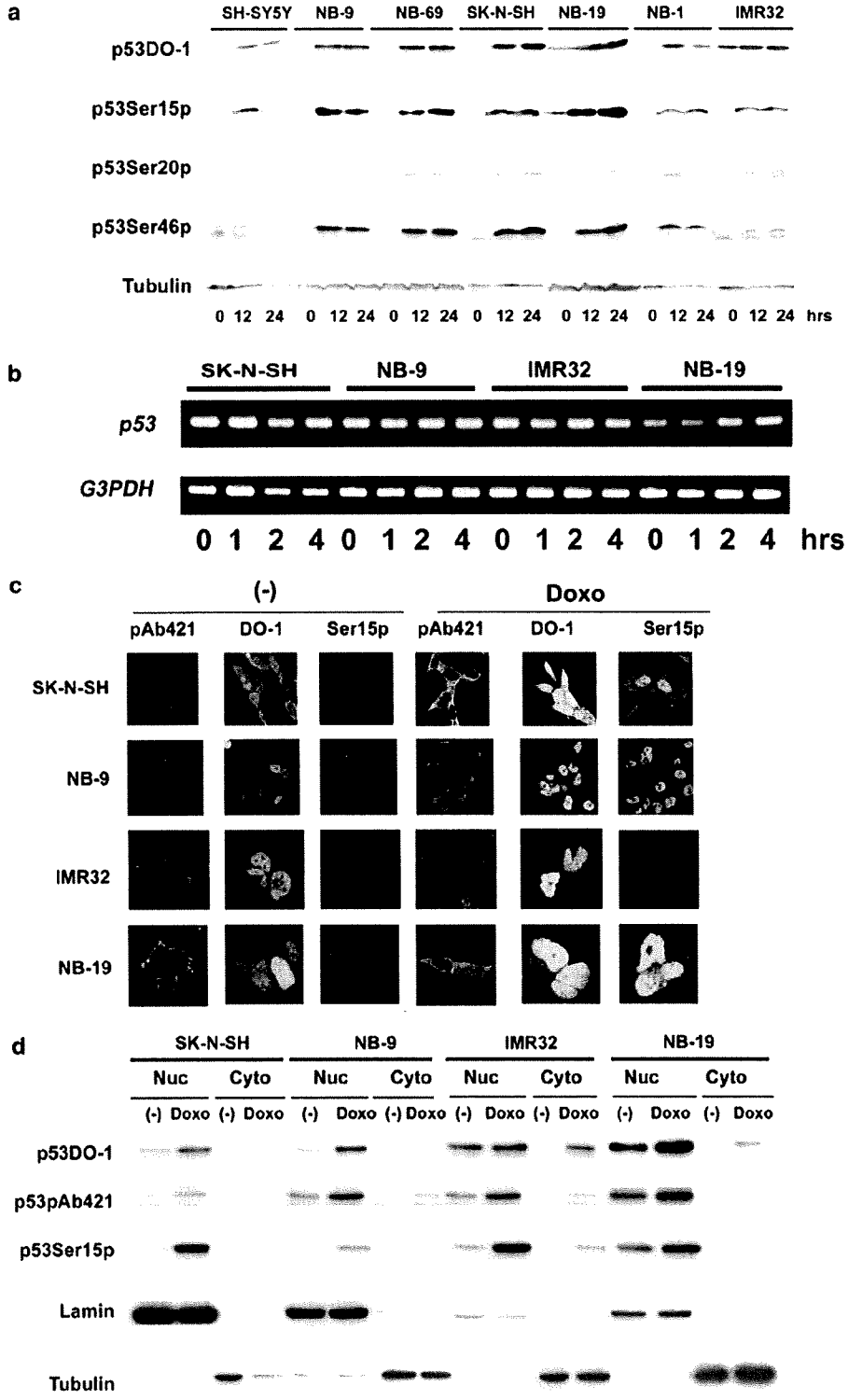

detected before treatment, the phosphorylation was remarkably upregulated by Doxo in SK-N-SH, NB-9 and NB-19 cells. In IMR32 cells, p53ser15 phosphorylation was modestly upregulated. The ser15-phosphorylated p53 accumulated to a much greater degree in the nucleus than in the cytoplasm after Doxo treatment. The use of several different fixation methods and modification of the first antibody concentration did not influence the results of immunofluorescence. Moreover, *p53* wild-type MCF7 cells showed similar staining results with these antibodies (data not shown). To investigate the observed discrepancy of p53 localization among the three monoclonal antibodies in the immunofluorescence experiments, we performed cell fractionation experiments (Figure 2d). All of the p53 signals were detected only in the nucleus before the treatment, and the upregulated signals induced by Doxo also accumulated in the nucleus rather than in the cytoplasm. The controls for fractionation, the nuclear marker lamin and cytoplasmic marker β-tubulin, were detected in the proper fractions and the amounts were not changed by Doxo treatment. These results show that the p53-dependent Doxo-stress increased the amount of p53 and induced the accumulation of p53 in the nucleus in both Doxo-sensitive and -resistant NB cells.

Activity of p53 as a transcriptional factor is required for Doxo-induced NB apoptosis

We then assessed the induction of p53-downstream molecules by Doxo. As shown in Figure 3a, exposure to Doxo induced remarkable $p21^{Cip1/Waf1}$ protein accumulation in the sensitive cells but not in the resistant cells, and this induction was caused at the transcriptional level (Figure 3b). HDM2 was similarly induced by Doxo treatment in the sensitive cells. However, *HDM2* mRNA accumulated in the resistant cells before Doxo treatment and did not change subsequently (Figure 3b), which is consistent with its protein accumulation (Figure 3a). These results indicate that the Doxo-induced cellular stress can effectively induce the p53 transcriptional activities in Doxo-sensitive NB cells but not in the resistant cells.

Doxo treatment induces synthesis of pro-apoptotic Noxa in the sensitive NB cells but not in the resistant cells

Next, we studied the expression of Bcl-2 family proteins in the NB cells, because regulation of the Bcl-2 family proteins by p53 is known to be the main component of p53-dependent apoptosis (Shen and White, 2001). The pro-apoptotic Bcl-2 family proteins Bax, Bak and Bok were not modified by Doxo in the NB cells (Figure 3a). Expression of Puma and p53AIP1 was also not affected by Doxo treatment (data not shown). It is interesting that Noxa was substantially induced only in the sensitive cells but not in the resistant cells. Although there was a considerable difference in the amount of anti-apoptotic Bcl-2 among the NB cells, its expression seemed not to be related to the Doxo sensitivity. The other anti-apoptotic Bcl-2 family protein Bcl-xL was not detected in any of the NB cells (data not shown). To assess whether the induction of Noxa is regulated at the transcriptional level, we performed semi-quantitative RT–PCR analysis. Consistent with the results of the western blot analysis, the mRNA amount of Noxa was clearly upregulated by Doxo treatment in the Doxo-sensitive SK-N-SH cells (Figure 3b). Meanwhile, the accumulation of *Noxa* mRNA expression was detected in the resistant cells (Figure 3b) and confirmed by quantitative real-time PCR analysis (Figure 3c). However, *Noxa* mRNA was not increased by Doxo treatment in the resistant cells (Figure 3b).

Noxa accumulation in mitochondria is not sufficient to induce apoptosis in NB cells

A recent report demonstrated that Noxa and Bok were induced by DNA stress dependent upon the p53 pathway in the SH-SY5Y cell line (Yakovlev *et al*., 2004). However, only Noxa upregulation was detected in the present study in the sensitive NB cell lines. Interestingly, larger amounts of Noxa were observed in the Doxo-resistant NB lines (IMR32 and NB-19) compared with the sensitive lines (SK-N-SH and NB-9). Since the organelle-specific amounts of the pro-apoptotic Bcl-2 family protein and its ratio to anti-apoptotic Bcl-2 family proteins in mitochondria are reported to determine cell fate in mitochondria-dependent apoptosis (Nakazawa *et al*., 2003; Danial and Korsmeyer, 2004), we studied the amounts of Noxa in mitochondria by cell fractionation/western blot analysis (Figure 4A). The amounts of Noxa in mitochondria were apparently upregulated in the sensitive cells. Densitometric analysis revealed that the Doxo-treatment increased the content of Noxa 10.3-fold in SK-N-SH cells and 16.6-fold in NB-9 cells compared to that before stimulation. On the other hand, Noxa was accumulated at higher levels in mitochondria of the resistant cells compared with the sensitive cells before Doxo treatment, and was not further increased by Doxo treatment. There were no significant differences in the amounts of Bcl-2 in the presence or absence of Doxo

Figure 2 Upregulation and nuclear accumulation of p53 in neuroblastoma (NB) cells. (**a**) Cells were collected after Doxo stimulation at the indicated time points (0, 12 and 24 h) and analysed by western blotting with the indicated antibodies (DO-1, p53ser15p, p53ser20p, p53ser46p and β-tubulin) as described in Materials and methods. (**b**) Cells were collected after Doxo stimulation at the indicated time points (0, 1, 2 and 4 h); p53 and G3PDH mRNA expression was analysed by RT–PCR as described in the Materials and methods section. (**c**) Cells were analysed by immunofluorescence with the indicated antibodies (pAb421, DO-1 and monoclonal anti-p53ser15p antibody: 16G8) 12 h after Doxo stimulation. (**d**) Cells were collected 12 h after Doxo stimulation and subjected to cell fractionation experiments as described in Materials and methods. Twenty micrograms of the proteins extracted from the organelle was analysed by sodium dodecyl sulfate–polyacrylamide gel electrophoresis (SDS–PAGE)/western blot experiments using the indicated antibodies. Lamin was used as a positive control for nuclear localization, and β-tubulin for cytosolic localization.

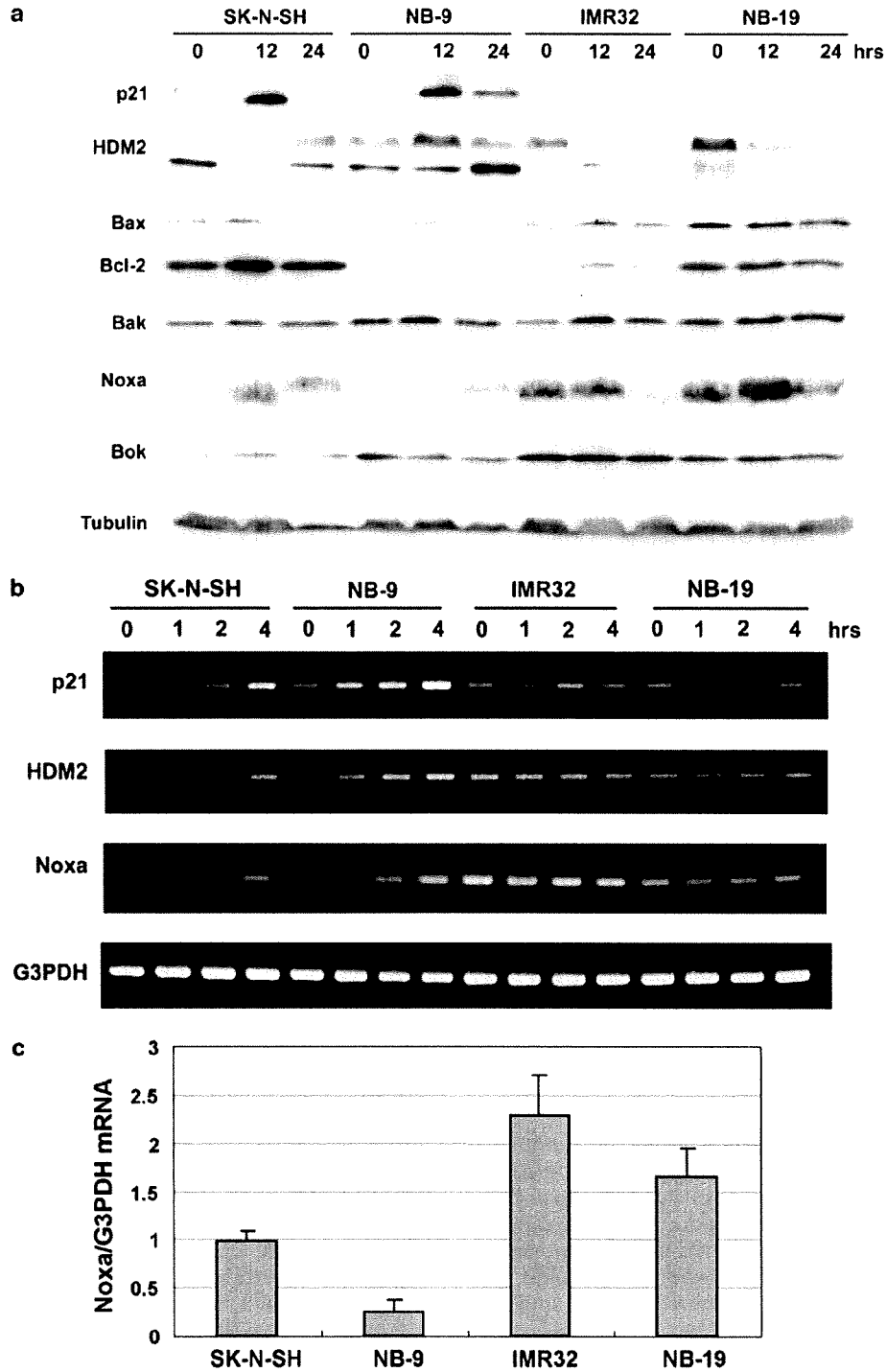

Figure 3 Modulation of p53-downstream proteins by Doxo treatment. The neuroblastoma (NB) cells were incubated with or without Doxo and collected at the indicated time points. (**a**) Extracted total cell lysates were subjected to sodium dodecyl sulfate–polyacrylamide gel electrophoresis (SDS–PAGE)/western blot analysis using the antibodies against the indicated molecules as described in Materials and methods. (**b**) Total RNA was subjected to semi-quantitative RT–PCR analysis as described in the Materials and methods section. (**c**) Quantitative real-time PCR analysis of *Noxa* mRNA amounts in NB cells as described in the methods section. Total RNA was extracted from unstimulated NB cells.

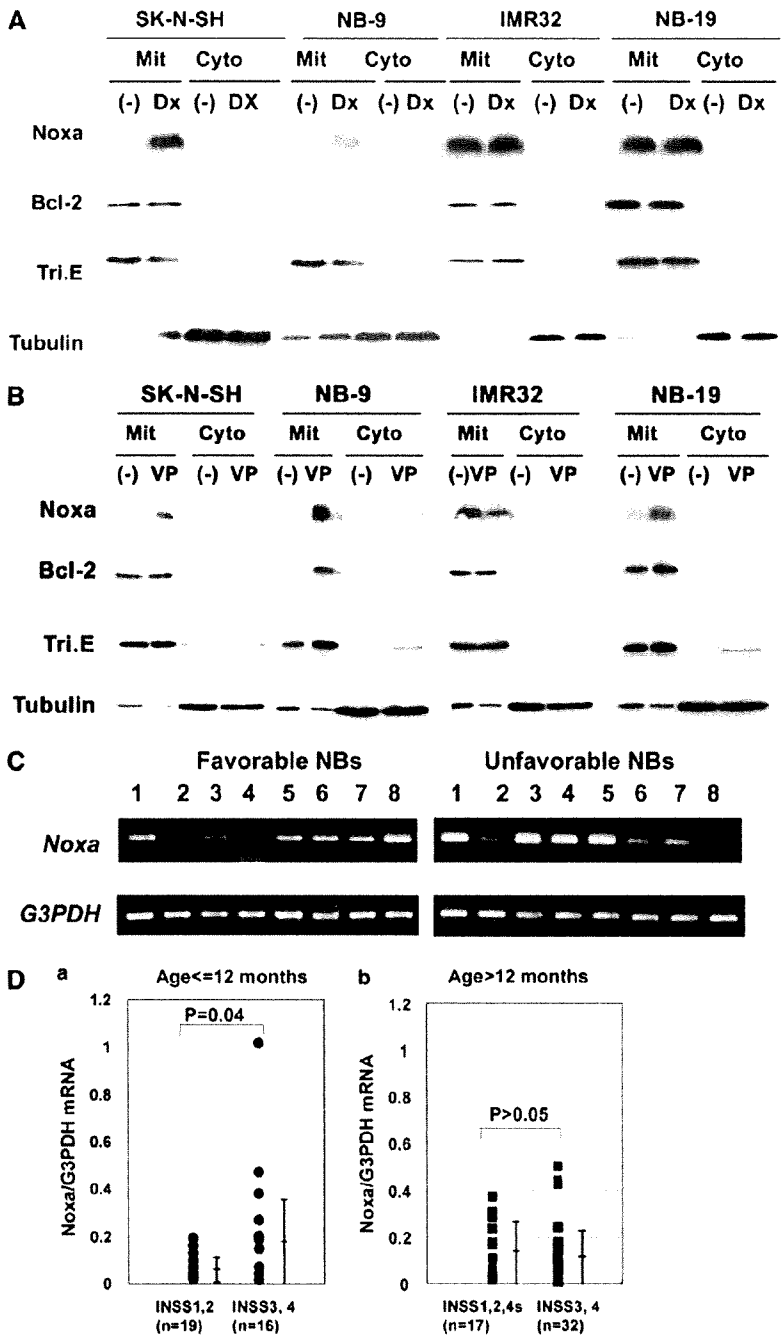

Figure 4 Noxa is upregulated in mitochondria by Doxo in the sensitive neuroblastoma (NB) cells. (**A** and **B**) Cells were collected 12 h after stimulation by Doxo (A, DX) or etoposide (B, VP) and subjected to cell fractionation for mitochondria (heavy membrane fraction: Mit) and the light membrane/cytosol fraction (Cyto). Samples were analysed by sodium dodecyl sulfate–polyacrylamide gel electrophoresis (SDS–PAGE)/western blotting with the indicated antibodies. Trifunctional protein (Tri E) and tubulin were controls for the mitochondrial fraction and cytosolic/light membrane fraction, respectively. This is a representative result of three independent experiments. (**C**) Semi-quantitative RT–PCR analysis of Noxa mRNA in favorable (stage 1 or 2, with single copy *MYCN*) and unfavorable (stage 3 or 4, with *MYCN* amplification) NB samples. (**D**) Quantitative real-time RT–PCR analysis of *Noxa* mRNA in 84 tumor samples from patients with NBs according to the tumor stage. The levels of Noxa were normalized to that of G3PDH. Results are presented as closed circles (**Da**) and closed squares (**Db**) with mean ± s.d. bars.

between the sensitive and resistant cells. Bcl-xL was not detected even by the fractionation experiments (not shown). The localization of trifunctional protein in mitochondria (Kamijo *et al.*, 1993) and β-tubulin in the cytosol confirmed the reliability of the fractionation procedures. Importantly, similar results on the Noxa kinetics in mitochondria were observed after the treatment by etoposide, the other p53-dependent damage-inducing anticancer drug in NB cells (Figure 4B). Consistent with the results of WST-8 assay (Figure 1b), Noxa upregulation in mitochondria was observed in etoposide-sensitive SK-N-SH, NB-9 and NB-19 cells but not in IMR32 cells. These results suggest that the ratio of pro- to anti-apoptotic molecules such as Noxa/Bcl-2 has a strong impact on the p53-dependent damage-induced apoptosis in NB cells.

Next, we assessed *Noxa* mRNA amounts in NB tumor samples by semi-quantitative RT–PCR (Figure 4C) and quantitative real-time reverse transcriptional (RT)–PCR (Figure 4D). Consistent with the upregulation of *Noxa* mRNA in the resistant cell lines (Figures 3b and c), some unfavorable NB samples expressed large amounts of *Noxa* mRNA (Figure 4C). Especially, high levels of *Noxa* mRNA expression were significantly associated with INSS3 and INSS4 samples that were younger than 12 months old ($P = 0.04$) according to the Welch test (Figure 4D). In the NB samples that were older than 12 months old, no obvious difference was detected, mainly due to the high expression of Noxa in INSS 1 samples. Although we checked the correlation of *MYCN* and *Noxa* mRNA expression, there was no significant correlation (data not shown).

Knockdown of Noxa effectively reduces Doxo-induced cell death in NB cells

To definitively establish a role of Noxa in Doxo-induced cell death in NB cells, both of the sensitive SK-N-SH cells and the resistant IMR32 cells were treated with *Noxa* small interfering RNA (siRNA) and then the NB cells had Doxo administered. Preincubation of the NB cells with the *Noxa* siRNA but not control siRNA effectively reduced the *Noxa* mRNA and also protein amounts in SK-N-SH cells (Figures 5a and b). Since the effectiveness of *Noxa* siRNA1 is better than that of *Noxa* siRNA2, we used *Noxa* siRNA1 for later experiments. The *Noxa* siRNA1 did not affect the pro-apoptotic Bcl-2 family molecules (Bax and Bak), an important inhibitor of apoptosis $p21^{Cip1/Waf1}$ and interferon-α (Figure 5c), suggesting that the knockdown seems to have a specific effect on Noxa. The ability of the *Noxa* siRNA to reduce the *Noxa* mRNA amounts was accompanied by a significant reduction in the

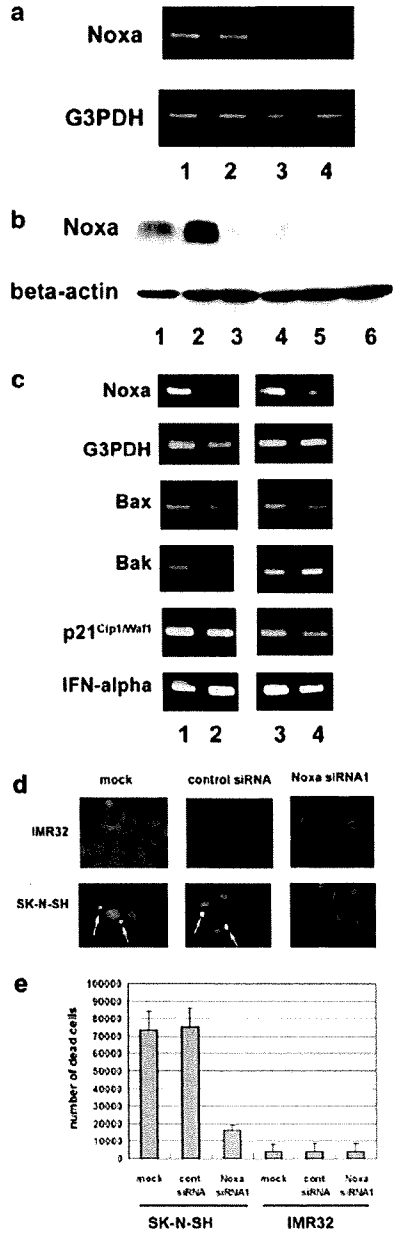

Figure 5 Noxa knockdown cancels Doxo-induced apoptotic cell death in sensitive neuroblastoma (NB) cells. (**a**) SK-N-SH cells were collected 48 h after small interfering RNA (siRNA) treatment (lane 1: mock; lane 2: control siRNA; lane 3: Noxa siRNA1; lane 4: Noxa siRNA2) and subjected to cDNA synthesis/semi-quantitative RT–PCR procedure. (**b**) SK-N-SH cells (lane 3: mock; lane 4: control siRNA; lane 5: Noxa siRNA1; lane 6: Noxa siRNA2) were collected 48 h after siRNA treatment and 30 μg of proteins was subjected to sodium dodecyl sulfate–polyacrylamide gel electrophoresis (SDS–PAGE)/western blot analysis. Lanes 1 and 2 were nontreated IMR32 and NB-19 cells, respectively, as controls. (**c**) Forty-eight hours after the siRNA treatment, cells were treated with 0.5 μg/ml Doxo. Twenty-four hours after Doxo administration, SK-N-SH (lanes 1 and 2) and IMR32 (lanes 3 and 4) cells were collected and subjected to cDNA synthesis/semi-quantitative RT–PCR for the analysis of the molecules indicated at the left side of panel. Lanes 1 and 3 are control siRNA treated, and lanes 2 and 4 are Noxa siRNA1 treated. (**d** and **e**) Forty-eight hours after the siRNA treatment, cells were treated with 0.5 μg/ml Doxo. Twenty-four hours after Doxo administration, the culture dish-attached SK-N-SH and IMR32 cells were stained with 4′,6-diamidino-2-phenylindole (DAPI) and nuclear morphology was analysed. The floating cells were collected and subjected to Trypan blue uptake analysis. Trypan blue-positive cells were counted as 'dead cells.'